










Ste20-like Kinase Is Critical for Inhibitory Synapse Maintenance and Its Deficiency Confers a Developmental Dendritopathy

 Susanne Schoch,^{1,2*}  Anne Quatraccioni,^{1*}  Barbara K. Robens,¹  Robert Maresch,³  Karen M.J. van Loo,^{1,5}  Silvia Cases-Cunillera,¹  Tony Kelly,³  Thoralf Opitz,³  Valeri Borger,⁴ Dirk Dietrich,⁴ Julika Pitsch,¹ Heinz Beck,³ and Albert J. Becker^{1*}

¹Institute of Neuropathology, Section for Translational Epilepsy Research, Medical Faculty, University of Bonn, Bonn, 53127, Germany,

²Department of Epileptology, University Hospital Bonn, Bonn, 53127, Germany, ³Institute of Experimental Epileptology and Cognition Research,

Medical Faculty, University of Bonn, Bonn, 53127, Germany, ⁴Department of Neurosurgery, University Hospital Bonn, Bonn, 53127, Germany, and

⁵Department of Epileptology, Neurology, RWTH Aachen University, Aachen, 52062, Germany

The size and structure of the dendritic arbor play important roles in determining how synaptic inputs of neurons are converted to action potential output. The regulatory mechanisms governing the development of dendrites, however, are insufficiently understood. The evolutionary conserved Ste20/Hippo kinase pathway has been proposed to play an important role in regulating the formation and maintenance of dendritic architecture. A key element of this pathway, Ste20-like kinase (SLK), regulates cytoskeletal dynamics in non-neuronal cells and is strongly expressed throughout neuronal development. However, its function in neurons is unknown. We show that, during development of mouse cortical neurons, SLK has a surprisingly specific role for proper elaboration of higher, \geq third-order dendrites both in male and in female mice. Moreover, we demonstrate that SLK is required to maintain excitation-inhibition balance. Specifically, SLK knockdown caused a selective loss of inhibitory synapses and functional inhibition after postnatal day 15, whereas excitatory neurotransmission was unaffected. Finally, we show that this mechanism may be relevant for human disease, as dysmorphic neurons within human cortical malformations revealed significant loss of SLK expression. Overall, the present data identify SLK as a key regulator of both dendritic complexity during development and inhibitory synapse maintenance.

Key words: dendrite; development; dysplasia; kinase; synapse assembly; synapse maturation

Significance Statement

We show that dysmorphic neurons of human epileptogenic brain lesions have decreased levels of the Ste20-like kinase (SLK). Decreasing SLK expression in mouse neurons revealed that SLK has essential functions in forming the neuronal dendritic tree and in maintaining inhibitory connections with neighboring neurons.

Received Feb. 15, 2021; revised May 18, 2021; accepted May 29, 2021.

Author contributions: S.S., K.M.J.v.L., T.K., T.O., D.D., J.P., H.B., and A.J.B. designed research; S.S., A.Q., T.K., H.B., and A.J.B. wrote the paper; A.Q., B.K.R., R.M., S.C.-C., and T.K. performed research; A.Q., B.K.R., K.M.J.v.L., T.K., T.O., D.D., and J.P. analyzed data; B.K.R. wrote the first draft of the paper; V.B. and A.J.B. contributed unpublished reagents/analytic tools.

*S.S., A.Q., and A.J.B. contributed equally to this work.

B. K. Robens' present address: Department of Neurology, F.M. Kirby Neurobiology Center, Division of Epilepsy and Clinical Neurophysiology and Epilepsy Genetics Program, Boston Children's Hospital, Harvard Medical School, Boston, Massachusetts.

This work was supported by Deutsche Forschungsgemeinschaft SFB 1089 to K.M.J.v.L., A.J.B., H.B., and S.S.; FOR2715 to H.B., T.K., and A.J.B.; and SCHO 820/4-1, SCHO 820/6-1, SCHO 820/7-1, SCHO 820/5-2, and SPP1757 to S.S.; BMBF 01GQ0806 to S.S.; University of Bonn Medical Center BONFOR program to A.J.B., S.S., K.M.J.v.L., and H.B.; DeCIPHER EraNet Neuron BMBF-Nr 01EW1606 to A.J.B. and H.B.; and Else Kröner-Fresenius Foundation EKFS-Promotionskolleg Neurolimmunology to A.J.B. Parts of this manuscript contributed to the PhD thesis of B.K.R.

The authors declare no competing financial interests.

Correspondence should be addressed to Susanne Schoch at susanne.schoch@uni-bonn.de or Albert J. Becker at albert_becker@uni-bonn.de.

<https://doi.org/10.1523/JNEUROSCI.0352-21.2021>

Copyright © 2021 the authors

Introduction

In the developing brain, neurons form intricately branched dendritic arbors. Their topology and morphology profoundly affect signal integration at dendrites (Mainen and Sejnowski, 1996; Schaefer et al., 2003; Ferrante et al., 2013). Usually, the extent of branching of the dendritic tree correlates with the number and distribution of competing excitatory and inhibitory inputs that the neuron can receive and process (Megias et al., 2001). This suggests that both the branching pattern of dendrites as well as dendritic synapse distribution must be precisely regulated (Katz et al., 2009; Warren et al., 2012; Kerrisk et al., 2013; Menon et al., 2013).

The dynamic and coordinated assembly and disassembly of the actin and microtubule cytoskeleton underlie dendritic outgrowth and branching and are regulated by the phosphorylation status of its components (Sfakianos et al., 2007; Arikath and

Reichardt, 2008; Jan and Jan, 2010). Several members of the Ste20/Hippo kinase family have been shown to be critically involved in the establishment of neuronal morphology and synapse formation, such as TAOK1/2, MINK, TNIK, MSN, and MST3b for spine synapse development in hippocampal cultures (Ultanir et al., 2014), and Hippo for dendritic tiling in *Drosophila* (Emoto et al., 2006). Ste20-like kinase (SLK) is a highly conserved mammalian member of the Ste20-kinase family with a pronounced expression in the developing brain (Zhang et al., 2002). SLK has been shown to control multiple aspects of cytoskeletal dynamics, including the orientation of microtubules, F-actin polymerization, and the actin–microtubule interplay in non-neuronal cells (Sabourin and Rudnicki, 1999; Sabourin et al., 2000; Wagner et al., 2002). In migrating fibroblasts, cross talk between actin and microtubules occurs at integrin- β 1 containing signaling complexes at the leading edge. A role for SLK in regulating the turnover of this complex has been suggested (Wagner et al., 2002). Therefore, in non-neuronal cells, SLK is a key regulator of growth and migration as well as of focal adhesion turnover (Sabourin and Rudnicki, 1999; Sabourin et al., 2000; Wagner et al., 2002, 2008; Quizi et al., 2013). Accordingly, constitutive SLK KO mice die during embryonic development and show marked developmental defects (Al-Zahrani et al., 2013, 2014). However, SLK's role in neurons, in particular during development, is still unresolved.

Here, we demonstrate a critical and highly selective role for SLK-mediated phosphorylation in regulating the formation of the distal compartment of the dendritic tree and the stability of inhibitory synapses. Functionally, this manifests in an impaired inhibition in SLK-deficient neurons. A loss of SLK in dysmorphic neurons of epileptogenic lesions indicates a potential role in human disease.

Materials and Methods

Ethical approvals. Informed and written consent for additional studies was given from patients included in this research project (for details, see Table 1). Procedures were conducted in accordance to the Helsinki Declaration and were approved by the local University of Bonn Medical Center ethics committee.

All animal studies were approved and performed in accordance to guidelines and regulations set forth by the local ethics committee and in accordance with the European Community Council Directive of November 24, 1986 (86/609/EEC). Animals were housed under controlled conditions (12 h light-dark cycle, temperature $22 \pm 2^\circ\text{C}$ and humidity $55 \pm 10\%$) with food and water *ad libitum*.

Cell culture and transfection procedures. HEK293T cells were cultured in DMEM (Invitrogen) supplemented with 10% FCS and 1% penicillin-streptomycin at 37°C in 5% CO_2 at a density of 70% confluency in 24-well plates. Cells were transfected 24 h later via calcium phosphate precipitation as described previously (van Loo et al., 2012; Grote et al., 2016) and harvested after 48 h.

Primary cortical neurons were dissected from E17-E19 mouse brains (van Loo et al., 2012; Alvarez-Baron et al., 2013; Grote et al., 2016) and plated at high density on poly-D-lysine-coated (0.01%) 24-well glass cover slips in NeuroBasal medium (Invitrogen) complemented with B27 and L-glutamine. Two to four days later (DIV2-DIV4), cortical neurons were transfected using calcium phosphate (Köhrmann et al., 1999; Grote et al., 2016) with either the SLK expression plasmids, the short hairpin RNA (shRNA) vectors alone or together with the shRNA-resistant rescue plasmids. For analysis of SLK's subcellular localization, mRFP and the expression regulated GFP-fused FingRs (fibronectin intrabodies generated with mRNA display) that bind to endogenous PSD95 or gephyrin with high affinity (pCAG_PSD95.FingR-eGFP-CCR5TC: AddGene plasmid #46 295 and pCAG_GPHN.FingR-eGFP-CCR5TC: AddGene

Table 1. Patient information^a

ID	Lesion	Age (yr) at surgery	Sex	Postsurgical outcome: ILAE classification	Medication with AED
1	GG	34	F	NA	NA
2	GG	9	M	1	No
3	GG	37	F	4	NA
4	GG	14	M	1	No
5	GG	38	M	1	Yes
6	GG	12	M	1	Yes
7	GG	17	F	3	NA
8	GG	31	M	3	NA
9	FCDIIb	48	M	1	NA
10	FCDIIb	4	F	1	NA
11	FCDIIb	71	M	1	No
12	FCDIIb	47	M	NA	NA
13	FCDIIb	44	M	3	Yes
14	FCDIIb	31	M	3	Yes
15	FCDIIb	20	M	NA	NA
16	FCDIIb	22	M	NA	NA
17	FCDIIb	20	M	5	NA
18	FCDIIb	33	F	NA	NA

^aSurgical tissue from GGs (WHO Grade I) and FCDIIb were obtained from male (M) and female (F) patients. ILAE, International League Against Epilepsy; AED, antiepileptic drugs.

plasmid #46 296 were a gift from Don Arnold (Gross et al., 2013) were cotransfected. Neurons were fixed in 4% PFA at DIV14 for dendrite number and immunolabeling experiments or at DIV21 for SLK localization analysis.

Adeno-associated virus (AAV) production. For recombinant AAV (rAAV2/8) production, HEK293T cells were grown to 80% confluency and plated onto 15 cm dishes (Greiner); 24 h later, the cells were transfected with the respective pAAV plasmid, helper plasmids encoding *rep* and *cap* genes (pRV1 and pH21), and adenoviral helper p Δ 6 using the calcium phosphate method. At 48–72 h after transfection, cells were lysed in 0.5% sodium deoxycholate (Sigma) and 50 U/ml Benzonase endonuclease (Sigma), and rAAV viruses were purified using HiTrap heparin column purification (GE Healthcare). rAAV particles were concentrated to a final volume of 400 μl by Amicon Ultra Centrifugal Filters (Millipore) (van Loo et al., 2015).

Protein separation and Western blot. Protein-expressing HEK293T cells were harvested in PBS 48 h after transfection and pelleted. Cells were resuspended in lysis buffer (4 mM HEPES, 150 mM NaCl, 1% Triton X-100, protease inhibitor cocktail (cComplete Roche)), sonicated for 2 s, and cell debris was pelleted. Protein concentration in the supernatant was determined at the NanoDrop (ND-100); 50 μg /sample was mixed with 6 \times Laemmli buffer (Tris-hydrochloride 378 mM, 30% glycerol, 12% SDS, 0.06% Bromophenol blue, 10% β -mercaptoethanol), denatured at 95°C for 5 min, and separated by SDS-PAGE. Afterward, proteins were transferred to a nitrocellulose membrane, which was blocked in 3% fish gelatin subsequently. Primary antibodies mouse anti- β -Actin (1:10,000, Abcam) and rabbit anti-SLK (1:800, generous donation by Prof. Luc Sabourin, Ottawa Hospital Research Institute) were incubated for 2–3 h at room temperature. After three washing steps, fluorescently labeled IRDye anti-mouse 800 nm or IRDye anti-rabbit 680 nm IgG (LI-COR) was incubated for 45 min in a dilution of 1:20,000 and detected with the infrared Odyssey system (LI-COR Biosciences). Band intensity was quantified with ImageJ.

Generation of constructs. cDNAs for mouse kinase-dead SLK (K63R; kindly provided by Prof. Luc Sabourin, Ottawa Hospital Research Institute), mouse SLK (mSLK), and mutated human shRNA-resistant SLK (hSLK) were amplified from plasmids and ligated into the pB-CAG-GFP and/or pB-CAG-mCherry plasmids kindly provided by Joe LoTurco (University of Connecticut) into XmaI and AgeI (mSLK) or EcoRI and AgeI (hSLK) restriction sites, respectively. Corresponding shRNAs were designed based on sequences in the RNAi Codex database (Olson et al., 2006), ordered as oligonucleotides from Invitrogen, and annealed in 100 mM Tris, pH 7.5, 1 M NaCl, and 10 mM EDTA solution for 10 min at 95°C . Afterward, samples were slowly cooled down to

Table 2. Cloning primers^a

Primers	5'-3' sequence
mSLK-GFP-fw	GCGCCGGGATGCTCTTCAATTTCCGTAAG
mSLK-GFP-rev	GCGACCGGTCTGACCCAGTGGAATGTAAG
mSLK-mCherry-fw	GCGCCGGGATGCTCTTCAATTTCCGTAAG
mSLK-mCherry-rev	GCGACCGGTCTGACCCAGTGGAATGTAAG
hSLK-GFP-fw	GCGGAATCACCATGCTCTTCAATTTCCGTAAGA
hSLK-GFP-rev	ACCGGTTGATCCGGTGAATGCAAGC
hSLK-mCherry-fw	GCGGAATCACCATGCTCTTCAATTTCCGTAAGA
hSLK-mCherry-rev	ACCGGTTGATCCGGTGAATGCAAGC
shRNA against SLK for pAAV plasmids: shSLK-fw	GATCTCGGGTTGAGATTGACATATTAATAGTGAAGCCACAGATGTATTAATATGCAATCTCAACCTTTGGAAA
shSLK for pAAV plasmids: shSLK-rev	AGCTTTCCAAAAGGTTGAGATTGACATATTAATACATCTGGCTTCACTATTAATATGCAATCTCAACCCGA
shSLK for pLVTHM plasmids: shSLK-fw	CGCTGGTTGAGATTGACATATTACTCGAGTAATATGCAATCTCAACCTTTTAT
shSLK for pLVTHM plasmids: shSLK-rev	CGATAAAAAAGGTTGAGATTGACATATTACTCGAGTAATATGCAATCTCAACCA

^aThe primer pairs were designed to clone constructs used in this study. fw, forward primer; rev, reverse primer.

room temperature and inserted into the vectors pAAV-U6-shRNA-CBA-hrGFP/pAAV-U6-shRNA-CBA-mRFP (rAAV; hrGFP; mRFP) or pLVTHM-mRFP (Lentivirus; mRFP) via BamHI and HindIII or MluI and ClaI restriction sites, respectively. All primer pairs, including restriction enzyme recognition sequences used in this study, are listed in Table 2.

Immunohistochemistry. For coimmunofluorescence analysis, brains from *in utero* electroporated and perfused mice were collected at postnatal day (P) 30–40 and cut to 80 μ m slices on a Microm HM 650V vibratome (Thermo Fisher Scientific). Afterward, brain slices were washed in 0.1% Triton X-100 PBS solution and blocked with 0.1% Triton X-100, 0.1% Tween 20, and 4% BSA in TBS, pH 7.7, for 1 h. This was followed by an overnight incubation with primary antibodies mouse anti-NeuN (1:300, Millipore), rabbit anti-GFAP (1:400, Sigma), or rabbit anti-SLK (1:800, generous donation by Prof. Luc Sabourin, Ottawa Hospital Research Institute) at 4°C. After three washing steps, brains were incubated with secondary fluorescently labeled antibodies AlexaFluor-647 and -405 (Invitrogen) for 1 h and mounted on glass slides with vectashield (Vector Laboratories).

For immunofluorescence analyses of ganglioglioma (GG) and focal cortical dysplasia Type IIb (FCDIIb) tissue diagnosed according to the current WHO classification by an experienced neuropathologist (A.J.B.) (Louis et al., 2007), we used paraffin sections. We identified tumor or lesion versus adjacent nontumor or nonlesioned “control” CNS tissue based on H&E staining. Paraffin was removed via a xylol-alcohol series. Afterward, the sections were microwaved for permeabilization in 0.1 M citric buffer for 20 min. Slices were then blocked in 10% FCS and 1% NGS in PBS for 2 h at 37°C, followed by an overnight incubation with primary antibodies mouse anti-microtubule-associated protein 2 (MAP-2) (1:400, Millipore), chicken anti-vimentin (1:2000, Millipore), and rabbit anti-SLK (1:800, generous donation by Prof. Luc Sabourin, Ottawa Hospital Research Institute) at room temperature. After washing 3 times with 0.1% Triton X-100 in PBS, sections were incubated for 2 h at 37°C with secondary antibodies AlexaFluor-647, -488, and -405 (1:200) and then mounted with corbit (Eukitt) mounting medium.

For immunofluorescence analysis of transfected primary cortical neurons at DIV14 or DIV21, cells were fixed with 4% PFA for 15 min, washed 3 times with PBS, incubated for 10 min with 0.3% Triton X-100, and subsequently treated with blocking solution (0.1% Triton X-100, 1% FCS, 10% BSA in PBS) for 1 h. Neurons were then incubated overnight with primary antibodies against mouse MAP-2 (1:200, Millipore) or SLK (1:800, generous donation by Prof. Luc Sabourin, Ottawa Hospital Research Institute) at 4°C. After washing with PBS, secondary antibodies against mouse AlexaFluor-405, rabbit AlexaFluor-647 (1:200), or AlexaFluor-488 phalloidin (1:300, phalloidin-iFluor 488, Abcam) were applied for 45 min at room temperature, followed by three washing steps.

Image analysis and quantification. Confocal images of single transfected primary neurons were acquired with a Nikon Eclipse Ti confocal microscope (Nikon Instruments) and subjected to morphometric analyses and quantification using ImageJ software with NeuronJ plug-in. Each traced branch of a DIV14 primary neuron was designated as primary,

secondary, or higher-order dendrite depending on its branch point origin. Neurites growing out of the neuron's soma were labeled as primary or first-order dendrites, dendrites branching from first-order dendrites were defined as secondary or second-order dendrites, and those branching from secondary dendrites accordingly as higher-order dendrites. The total number of primary, secondary, and higher-order dendrites was then calculated for each neuron in each condition and summarized as mean value. The length of each branch was determined using the NeuronJ plug-in of ImageJ after reconstruction of the neuronal arbor.

Confocal maximum intensity projection images of *z* stacks of coimmunohistochemically stained GG or FCDIIb samples were analyzed by NIS Elements Nikon software. With the auto-detect function, all MAP-2-expressing neurons were automatically recognized and set as an ROI inside or outside the region of the GG (visualized by strong vimentin immunoreactivity). For FCDIIb analysis, dysmorphic neurons with dramatically increased soma size and strong MAP-2 immunoreactivity were analyzed. As controls, we analyzed normal-sized neurons without apparent pathologic change of morphology in an area with maximal distance from dysmorphic neurons. Single-cell SLK fluorescence intensity was determined by the software within the ROI for semiquantitative SLK protein expression in lesioned and control tissue and subtracted by background fluorescence of individual micrographs.

After *in utero* electroporation (IUE) or viral injections, 80 μ m coronal vibratome brain slices were analyzed. For Sholl analysis and quantification of total dendrite number, confocal images were taken and each branch from single hrGFP/mRFP-expressing neurons was traced from the branching point to the tip using NeuronJ or Imaris 9.1.0. Primary, secondary, and higher-order dendrites were determined as described before. Each traced neuron was overlaid with rings in 10/1 μ m intervals, and the number of intersecting neurites was counted for each circle by the Sholl analysis ImageJ Plug-In or the Imaris software (Sholl, 1953). In order to analyze single *in utero* electroporated or transduced neurons, mostly isolated multipolar neurons from cortical layers 2/3 at the borders of the IUE or injection area were selected. Robust overexpression of a kinase-dead SLK K63R-mRFP/GFP variant by IUE, assayed by red or green fluorescence, was for unknown reasons not possible.

After *in utero* co-electroporation of shSLK-mRFP or the empty shRNA vector together with GFP-fused FingRs, synapse density of proximal dendrites was determined in mice of different ages. Neurons were analyzed by manually counting all green punctae overlapping with the volume dye mRFP. Afterward, the length of the processes was analyzed with NeuronJ software. The corresponding number of gephyrin⁺ or PSD95⁺ punctae per dendrite was summarized as the mean value per 100 μ m dendrite.

Confocal maximum intensity projection images of *z* stacks of transfected primary cultured cortical neurons were taken to analyze possible overlap of SLK immunolabeling with PSD95- or gephyrin-GFP-FingR expression. We performed background correction by subtracting the corresponding background fluorescence intensity from the SLK, gephyrin-GFP, or PSD95-GFP fluorescence signal. We defined an overlap as positive or colocalized if the PSD95- or gephyrin-GFP ROI overlapped with SLK, with >3 times the fluorescence intensity of the

background; all SLK fluorescence intensity values <3 times the value of the background were counted as negative or not colocalized.

All images and figures were edited and created in Adobe Photoshop CS5/CS6 or Adobe Illustrator CS5/CS6.

IUE in mice. Intraventricular IUE used in our laboratory was described previously (Grote et al., 2016). In short, time pregnant CD1/C57BL/6 WT mice (embryonic day [E] 14) were deeply anesthetized with isoflurane inhalation and injected with gabrilen (5 mg/kg, Mibe) and buprenovet (0.05 mg/kg, Bayer) as analgesia. Uterine horns were exposed from the abdominal cavity, and each embryo was injected once into the lateral ventricle with 1–2 μ l DNA (with a concentration of 1.5 μ g/ μ l) and Fast Green (1 mg/ml, Sigma) with a pulled and beveled glass capillary (Drummond Scientific) using a microinjector (Picospritzer III, General Valve). Five electric pulses with 50 ms duration were delivered at 950 ms intervals with a 7 mm electrode by discharging a 4000 μ F capacitor charged to 45 V with a CUY21SC electroporator (Nepa Gene). Electrode forceps were placed to target cortical ventricular progenitors in the somatosensory and motor cortex (Saito and Nakatsuji, 2001). Five, 15, 30, 45–50, or 60 d after birth, electroporated animals were anesthetized with ketamine/xylazine (100 mg/kg and 10 mg/kg, respectively) and killed by cardiac 4% PFA perfusion. *In utero* electroporated offspring mice were assigned to experimental groups based on the electroporated plasmids regardless of sex.

Stereotactic viral vector injection. For intracortical viral injections, mice at P30–P32 were anesthetized with fentanyl (0.05 mg/kg, Braun) + midazolam (5 mg/kg, Braun) + medetomidin (0.5 mg/kg, Zoetis) intraperitoneally, and holes were drilled into the skull at the coordinates (in mm) as follows: 1 posterior, $-0.9/0.9$ lateral, and 1.5 ventral relative to bregma. Using a 10 μ l Hamilton syringe, stereotactic injection of 300 nl virus was performed into both hemispheres at 3 depths (1.5/1/0.5 ventral) at a rate of 200 nl/min, regulated by a microprocessor-controlled mini-pump (World Precision Instruments). Five minutes after the injection, the needle was withdrawn and the incision site closed.

Electrophysiological approaches. Mice ranging from 4 to 6 weeks in age were decapitated under deep isoflurane anesthesia. The brain was quickly removed and immersed in ice-cold preparation solution of the following composition (in mM): NaCl 60, sucrose 100, KCl 2.5, CaCl_2 1, MgCl_2 5, NaH_2PO_4 1.25, D-glucose 20, NaHCO_3 26, pH 7.4, when saturated with 5% $\text{CO}_2/95\%$ O_2 . 300- μ m-thick coronal brain slices containing the somatosensory cortex were prepared with a vibratome (Microm HM650 V, Thermo Fisher Scientific). After slowly warming the slices to 35°C in preparation solution over 20 min, slices were kept until recording at room temperature in aCSF of the following composition (in mM): NaCl 125, KCl 3, CaCl_2 2, MgCl_2 2, NaH_2PO_4 1.25, D-glucose 15, NaHCO_3 26, pH 7.4, when saturated with 5% $\text{CO}_2/95\%$ O_2 .

Two-photon imaging and cell identification. Cells were visualized using an Eclipse FN1 upright microscope equipped with infrared difference interference contrast optics and a water-immersion lens ($\times 60$, 0.9 NA; Olympus). Two-photon laser irradiation at 810 nm was provided by a Ti:Sapphire ultrafast-pulsed laser (Chameleon Ultra II, Coherent) and a galvanometer-based scanning system (Prairie Technologies). Fluorescent emissions were separated using a dichroic mirror (DXC 575). Green hrGFP fluorescence was collected at 525/70 nm. Cells electroporated with shSLK-hrGFP or hrGFP control plasmids were identified visually by hrGFP fluorescence, and targeted whole-cell patch-clamp recordings were obtained. Cells were filled with Alexa-594 via the pipette, and fluorescence was collected at 605/45 nm.

Voltage clamp. Miniature EPSCs and IPSCs (mEPSCs and mIPSCs, respectively) were recorded under whole-cell voltage-clamp conditions from neurons within cortical layer 2/3 with a pyramidal morphology. Somatic whole-cell voltage-clamp recordings were made with an AxoPatch 200B amplifier (Molecular Devices). Data were sampled at 10 kHz and filtered at 1 kHz with a Digidata 1322A interface controlled by pClamp software (Molecular Devices). Electrode resistance in the bath ranged from 3 to 4 $\text{M}\Omega$, and series resistance ranged from 8 to 27 $\text{M}\Omega$. The internal solution contained the following (in mM): cesium methanesulfonate 110, tetraethylammonium chloride 10, HEPES 10, EGTA 11, CaCl_2 2, Mg-ATP_2 2, Alexa-594 100 μM , pH adjusted to

7.2 with CsOH (290 mOsmol). The extracellular solution contained the following (in mM): NaCl 140, KCl 3.5, CaCl_2 2, MgCl_2 1, D-glucose 25, HEPES 10, and TTX 300 nM, pH adjusted to 7.4 with NaOH (310 mOsmol). Potentials were corrected offline for a liquid junction potential of 10 mV.

Passive membrane properties were quantified as follows. The input resistance was determined under voltage-clamp conditions from the steady-state current responses to 5 or 10 mV voltage steps (200 ms) from a -77.5 mV holding potential and was not significantly different between the hrGFP and shSLK-hrGFP group. Holding currents in both groups were not significantly different (-108.9 ± 9.4 pA, $n = 12$, and -101.1 ± 8.5 pA, $n = 11$). Cell capacitance was determined as the charge (Q_c) required to fully charge the membrane. Q_c was measured as the total area under the current response to the aforementioned voltage steps, minus the charge flowing across the membrane resistance. Cell capacitance was then calculated as Q_c/V , where V was the amplitude of the voltage step. Frequencies and amplitudes of mEPSCs were determined at a holding potential of -67 mV, which was the calculated Cl^- reversal potential at 35°C. mEPSCs were measured for 2 min. Subsequently, the cell was clamped to 0 mV, and mIPSCs were recorded for 30 s. Offline detection and analysis of mEPSCs and mIPSCs were performed with a custom routine programmed in IGOR Pro. Detection of mEPSC events was performed by calculating the first derivative of current traces and selecting events for which the first derivative was >5 times the SD of the baseline 0–3 ms before the event. An additional criterion used for mEPSCs was that the mEPSC time constant of decay had to be between 5 and 15 ms. mIPSCs were detected if the difference between the mean current amplitudes in two adjacent moving windows (0.5 ms) was >5 pA. All detected postsynaptic currents were assessed by visual inspection and events because of spurious noise were rejected manually.

Active properties. Active action potential (AP) properties were determined under current-clamp conditions; subsequently, the paired-pulse ratio (PPR) was determined in voltage-clamp mode in the same cell. These current-clamp and paired pulse-experiments were conducted using a BVC.700A amplifier (Dagan). Data were sampled at 100 kHz and filtered at 10 kHz with a Digidata 1322A interface controlled by pClamp software (Molecular Devices). Electrode resistance in the bath ranged from 3 to 4 $\text{M}\Omega$, and series resistance ranged from 8 to 27 $\text{M}\Omega$. The internal solution contained the following (in mM): potassium-glucuronate 140, HEPES acid 5, EGTA 0.16, MgCl_2 0.5, phosphocreatine-disodium 5, Alexa-594 100 μM , pH adjusted to 7.25 with KOH (290 mOsmol). The extracellular solution contained the following (in mM): NaCl 125, KCl 3, NaH_2PO_4 1.25, NaHCO_3 26, CaCl_2 2, MgCl_2 2, glucose 15, pH adjusted to 7.4 with NaOH (308 mOsmol). Holding potentials were corrected offline for a liquid junction potential of 15 mV.

Under these recording conditions, the resting membrane potential [mV] was -75.7 ± 1.9 ($n = 8$, control [hrGFP]) and -72.8 ± 1.6 ($n = 12$, shSLK-hrGFP), input resistance [$\text{M}\Omega$] was 179.3 ± 13.2 and 230.7 ± 42.9 , and cell capacitance [pF] was 144.2 ± 8.1 and 133.8 ± 18.9 , respectively. The input-output relationship was determined using 500 ms depolarizing current injections to elicit trains of APs. Individual APs were elicited by 500 ms current injections and AP properties measured from the first AP elicited within 20 ms of the current injection (Ferrante et al., 2013). The peak potential was the maximum voltage attained, amplitude determined as the difference from AP threshold. The AP duration was determined as the duration at the half-maximal amplitude. The maximal depolarization and repolarization rates were the high and low points of the first derivation of the voltage trace. AP threshold was determined from the peak of the second derivative (Thome et al., 2014). The fast afterhyperpolarization amplitude was the difference between the maximum hyperpolarization reached within 5 ms of the AP and the AP threshold.

The PPR was quantified at different interstimulus intervals (50–300 μA) as the amplitude ratio of IPSC2/IPSC1. For stimulation, a concentric bipolar electrode (FHC) was placed laterally at a distance of 70–250 μm from the recorded cell in layer 2/3. The membrane voltage was held at -60 mV, and CNQX and D-AP5 (10 and 25 μM , respectively) were included in the bath solution to block glutamatergic transmission.

Experimental design and statistical analysis. In this study, male and female mice were used in both the experimental and the control groups. Sample sizes and the appropriate controls are indicated in the figure legends. The following statistical tests were applied: repeated-measures two-way ANOVA with Sidak's multiple-comparisons test (dendrite number and length *in vitro*, dendrite number and Sholl analysis *in vivo*; see Figs. 1 and 2), one-way ANOVA with Sidak's multiple-comparisons test (Western blot analysis; see Fig. 1), two-way ANOVA with Sidak's multiple-comparisons test (dendrite number *in vivo*, PPR, and number of APs; see Fig. 4), two-way ANOVA with Tukey's multiple-comparisons test (synapse quantification *in vivo*; see Fig. 4), and unpaired two-tailed *t* test (electrophysiological measurements and SLK fluorescence quantification in dysmorphic neurons; see Figs. 4 and 5). Details about test statistics and degrees of freedom (for ANOVA as $df = DfN, DfD$) can be found in the figure legends. All SEs are indicated as the SEM. Statistical analyses were performed with Prism GraphPad (version 6.07).

Results

SLK is required for establishing higher-order dendrites *in vitro*

To examine whether a decrease of SLK protein levels affects neuronal development, we generated specific shRNAs targeted against mSLK mRNA sequences as well as shRNA-resistant human cDNA variants (hSLK) for rescue experiments. We confirmed knockdown and rescue efficiency by immunoblotting of protein homogenates from HEK293T cells, which had been cotransfected with the mSLK MCherry-tagged expression plasmids, the hrGFP-expressing shRNA, and the shSLK-resistant hSLK rescue plasmid (Fig. 1A). In addition, SLK staining of shSLK-expressing neurons *in vitro* confirmed that SLK protein levels were reduced compared with control neurons (Fig. 1B).

We then used the validated shRNA to reduce the expression of SLK in primary cortical neurons (DIV4) with the plasmid coding for shSLK and hrGFP (shSLK-hrGFP). As a control, neurons were transfected with the empty shRNA vector only expressing hrGFP. The neuronal morphology was analyzed at DIV14 using confocal micrographs (Fig. 1C). While proximal first- and second-order dendrites were not altered in the absence of SLK, the number of higher-order dendrites was significantly reduced by 41.2% on SLK loss (control [hrGFP] 30.8 ± 2.1 vs shSLK-hrGFP 18.1 ± 1.5 higher-order dendrites per neuron), or by 39.3% on expression of the kinase-dead SLK K63R mutant (18.7 ± 2.1 higher-order dendrites per neuron). Coexpression of shRNA-resistant hSLK reversed the decrease of higher-order dendrites to levels that were even higher than those in hrGFP-expressing control neurons (43.6 ± 1.5 higher-order dendrites per neuron; Fig. 1D). None of the tested conditions caused a significant change in the average length of individual first-, second-, or higher-order dendrite segments compared with control (Fig. 1E). These results demonstrate a selective role of SLK in the formation of the distal dendritic tree.

Impairment of cortical development after shRNA-mediated SLK knockdown *in vivo*

We next probed whether reducing SLK expression in developing neurons *in vivo* also causes similar changes in dendritic morphogenesis. Mice were *in utero* electroporated at E14 with the validated shRNA (shSLK-hrGFP) or the control plasmid (hrGFP) (Fig. 2A). IUE of shSLK at E14 knocks down SLK in progenitor populations from cortical layers 2/3 and 4 (Fig. 2B) (Molyneux et al., 2007). At the time point of analysis on postnatal day P30-P35, neurons expressing hrGFP, indicating shSLK or hrGFP control vector expression, were spread throughout the somatosensory, agranular insular, dysgranular insular, and partly the motor

and cingulate cortex, ranging approximately from bregma 2.0 to -2.5 (Fig. 2B). Nonelectroporated cortical neurons showed moderate SLK immunoreactivity, which was absent in shSLK-expressing neurons and could be rescued by coexpression of the shRNA-resistant hSLK variant (Fig. 2C). In shSLK-electroporated mice, the cortical architecture was locally disrupted in electroporated brain areas. We found a subset of cells, varying in number, located in deeper cortical layers and identified them as ectopic neurons (Fig. 2D). GFAP staining was inconspicuous and did not show any differences between hrGFP control and shSLK-hrGFP electroporated animals (Fig. 2D). Subsequently, we selected single *in utero* electroporated neurons at the edge of the electroporated cortical area to further study their morphology (Fig. 2E,F). In accordance with the *in vitro* results, reduction of SLK protein levels by shSLK expression *in vivo* caused a significant and selective reduction in the number of secondary and higher-order dendrites (Fig. 2G; reduction of secondary dendrites by 24.3%, control [hrGFP] 17.7 ± 1.2 vs shSLK-hrGFP 13.4 ± 1.4 , and for higher-order dendrites by 62.5%, control [hrGFP] 9.3 ± 0.8 vs shSLK-hrGFP 3.5 ± 0.7 higher-order dendrites per neuron). This selective loss in complexity of the distal dendritic tree was also revealed by morphometric Sholl analysis (Fig. 2H). Thus, SLK is also essential *in vivo* for proper formation of the distal dendritic arbor.

To investigate whether SLK is required for the outgrowth and/or the maintenance of higher-order dendrites, we examined the effect of SLK knockdown in adult animals. However, intracortical injection of mRFP or shSLK-mRFP-expressing rAAV at P30-P32 (Fig. 2I,J) did not reduce the number of distal dendrites (Fig. 2K) or the complexity of the dendritic arbor at P74 (Fig. 2L). This finding shows that SLK is selectively required for the development of normal dendritic complexity but not for the maintenance of an established dendritic tree.

SLK is present in dendrites and inhibitory synapses

Our data so far show the importance of SLK in dendrite development, but it is still unresolved how SLK regulates this process and which cellular signaling complexes are involved. To this end, we first aimed at elucidating the subcellular distribution of SLK in neurons, which is still unknown. In non-neuronal cells, SLK has been shown to colocalize with the microtubule network during adhesion and spreading (Wagner et al., 2002). Therefore, the subcellular localization and potential colocalization with actin and dendritic microtubules were analyzed in cultured primary cortical neurons (DIV14). Neurons expressing mRFP as volume dye were labeled with antibodies against SLK and either the dendritically enriched MAP-2 or Alexa488-labeled phalloidin to visualize F-actin. SLK protein was present throughout the neuron, with a particularly strong expression in the cell body and in neurites where it colocalized with the dendritic marker protein MAP-2 (Fig. 3A). Remarkably, a prominent colocalization of SLK and phalloidin was detected in neurite tips/growth cones of mRFP-transfected neurons (Fig. 3B,C), supporting a functional role of the kinase in dendritic growth.

Synaptic localization and function have been reported for several other members of the Ste20 kinase family (TAO1/2, MST3, and TNIK) (Hussain et al., 2010; Ultanir et al., 2014; X. Chen et al., 2018). Next, we therefore assessed whether SLK is present at excitatory (PSD95⁺) or inhibitory (gephyrin⁺) synapses by transfecting neurons with a volume dye (mRFP) and the expression-regulated GFP-fused PSD95- or gephyrin-FingRs. SLK was detected at high levels evenly distributed throughout the dendrites but appeared to be absent from dendritic spines.

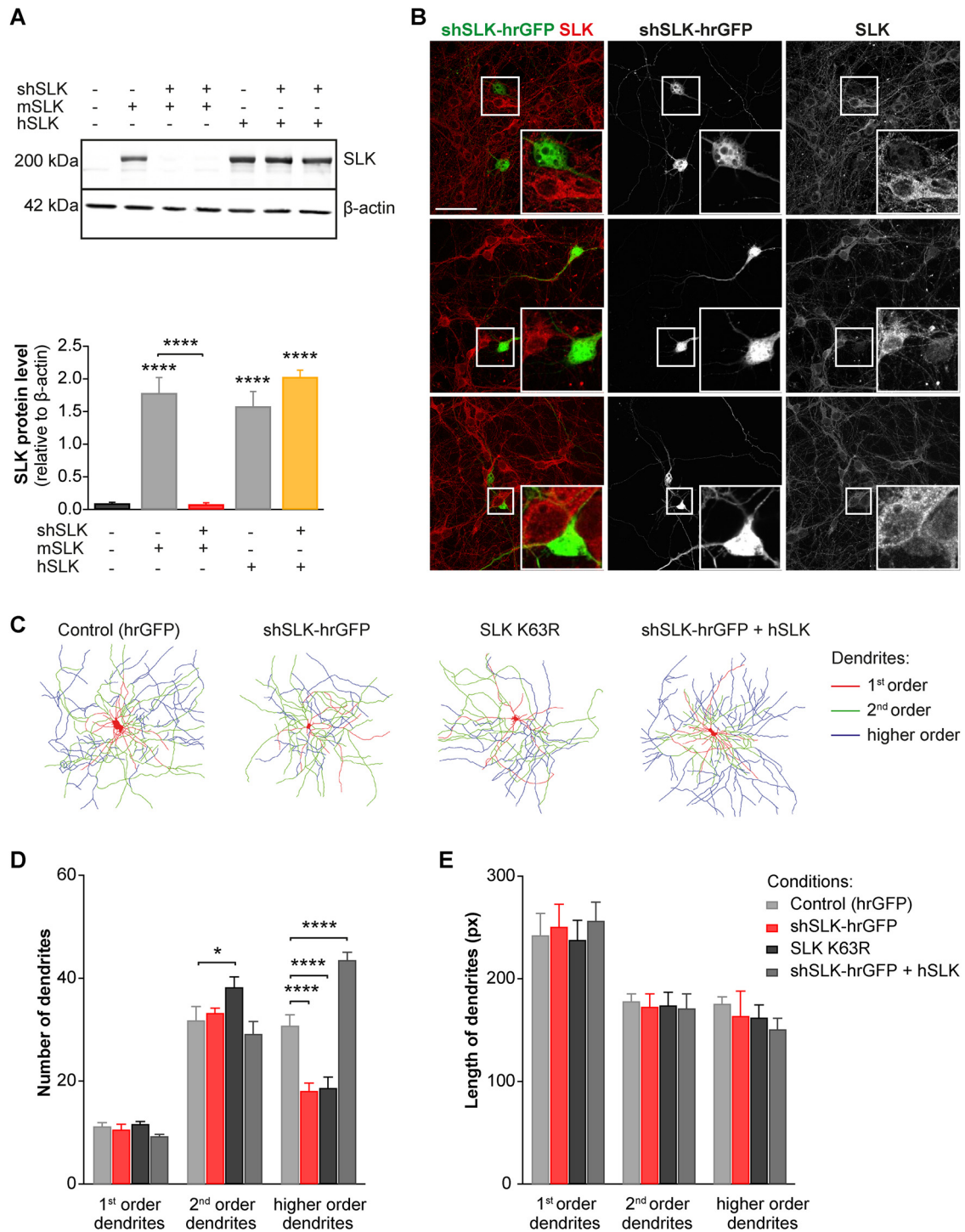


Figure 1. *In vitro* knockdown of SLK results in impaired dendritic arbor formation. **A**, HEK293T cells were transfected with SLK expression plasmids alone or together with mouse-specific shSLK. As a rescue, shSLK was introduced together with an shRNA-resistant hSLK variant. shSLK targeting mSLK specifically knocked down mouse SLK expression, whereas the expression levels of the shRNA-resistant hSLK were not affected. $n = 5$. One-way ANOVA (Conditions: $p_{(F=38.1; df=4, 20)} < 0.0001$); Sidak's multiple-comparisons test, **** $p < 0.0001$, compared with nontransfected control if not indicated otherwise (in detail: nontransfected vs mSLK: $p_{(t=7.753, df=20)} < 0.0001$; nontransfected vs mSLK + shSLK: $p_{(t=0.06797, df=20)} > 0.9999$; nontransfected vs hSLK: $p_{(t=6.822, df=20)} < 0.0001$; nontransfected vs hSLK + shSLK: $p_{(t=8.891, df=20)} < 0.0001$; mSLK vs mSLK + shSLK: $p_{(t=7.821, df=20)} < 0.0001$; hSLK vs hSLK + shSLK: $p_{(t=2.069, df=20)} = 0.2730$). **B**, Mouse cortical neurons were transfected on DIV2 with shSLK-hrGFP and stained with antibodies against SLK on DIV5. SLK expression was strongly reduced in shSLK-expressing neurons compared with nontransfected neighboring neurons. Scale bar, 50 μ m. Insets represent single neurons in a higher magnification. **C**, Neurons were transfected at DIV4 with an hrGFP control plasmid, shRNAs targeting SLK (shSLK-hrGFP), a kinase-dead SLK mutant (SLK K63R), or shSLK in combination with shRNA-resistant SLK expression plasmids (hSLK), and were reconstructed at DIV14. Color code indicates different order dendrites. **D**, Knockdown of SLK led to a significant reduction in the number of higher-order dendrites but no obvious change in the abundance of proximal processes. A similar effect was observed when kinase-dead SLK was transfected. Overexpression of shRNA-resistant hSLK counteracted the decrease in the total number of distal dendrites. $n = 10$ control (hrGFP), $n = 9$ shSLK-hrGFP, $n = 12$ SLK K63R, and $n = 11$ shSLK-hrGFP + hSLK neurons. Experiment was repeated 3 times; repeated-measures two-way ANOVA (Interaction: $p_{(F=28.88; df=6, 76)} < 0.0001$; Dendrite order: $p_{(F=22.11; df=2, 76)} < 0.0001$; Condition: $p_{(F=6.185; df=3, 38)} = 0.0016$); Sidak's multiple-comparisons test, * $p < 0.05$, **** $p < 0.0001$, compared with control (in detail: Primary dendrites: control vs shSLK: $p_{(t=0.2547, df=114)} = 0.9919$; control vs SLK K63R: $p_{(t=0.1979, df=114)} = 0.9962$; control vs shSLK + hSLK: $p_{(t=0.8009, df=114)} = 0.8097$; Secondary dendrites: control vs shSLK: $p_{(t=0.5621, df=114)} = 0.9233$; control vs SLK K63R: $p_{(t=2.735, df=114)} = 0.0215$; control vs shSLK + hSLK: $p_{(t=1.088, df=114)} = 0.6250$; Higher-order

Accordingly, a quantitative analysis revealed only a low degree of colocalization ($28.4 \pm 15.1\%$) of SLK and PSD95-GFP, which was concentrated at the tips of dendritic spines (Fig. 3D,E). In contrast, SLK was present at most inhibitory postsynaptic sites, as evidenced by a high degree of overlap with gephyrin⁺ punctae located on dendritic shafts ($97.7 \pm 1.8\%$; Fig. 3F,G). Together, these findings are consistent with SLK being present at inhibitory, but not excitatory, synapses.

SLK deficiency leads to a selective loss of inhibitory postsynapses *in vivo*

To further probe for a specific synaptic role of SLK restricted to inhibitory synapses, we analyzed whether SLK knockdown preferentially affects the density of inhibitory synapses compared with excitatory synapses. We *in utero* co-electroporated mice (E14) with the empty shRNA vector expressing mRFP as a control or shSLK-mRFP plasmids and expression-regulated GFP-fused PSD95/gephyrin-FingRs to label excitatory or inhibitory synapses (Fig. 4A,B). As higher-order dendrites were substantially reduced in number, we restricted our comparative analysis of synapse density in control versus SLK knockdown neurons to proximal dendrites. We found no significant changes in the density of excitatory postsynapses labeled with PSD95-FingRs at any time point (Fig. 4C). Quantification of gephyrin⁺ punctae showed that there was also no difference in the initial formation of inhibitory postsynapses between mRFP control and shSLK-mRFP neurons. After P15, however, inhibitory postsynapse density did not further increase as in mRFP control cortices, but instead displayed a significant decrease (Fig. 4D; gephyrin⁺ synapses/100 μm at P5: control [mRFP] 6.6 ± 0.7 vs shSLK-mRFP 4.7 ± 0.6 ; P15: control [mRFP] 16.5 ± 1.3 vs shSLK-mRFP 17.2 ± 0.7 ; P30: control [mRFP] 22.8 ± 2.0 vs shSLK-mRFP 13.1 ± 1.0 ; P60: control [mRFP] 25.6 ± 2.5 vs shSLK-mRFP 11.7 ± 1.0). Interestingly, this selective reduction of inhibitory postsynapses after P15 is preceded by the failure of SLK-deficient, developing neurons to form higher-order dendrites (Fig. 4E, no higher-order dendrites at P5; higher-order dendrites/neuron: P15: control [mRFP] 6.6 ± 0.9 vs shSLK-mRFP 1.1 ± 0.4 ; P30: control [mRFP] 9.3 ± 0.8 vs shSLK-mRFP 3.5 ± 0.7 ; P60: control [mRFP] 7.6 ± 1.1 vs shSLK-mRFP 2.3 ± 0.4). These results point to a role of SLK in regulating dendrite outgrowth as well as inhibitory postsynapse maturation and maintenance *in vivo*, culminating in a profoundly disturbed balance between dendritic excitation and inhibition.

Reduced inhibition in SLK knockdown neurons

In order to assess the functional consequences of SLK loss, we performed patch-clamp recordings in acute brain slices from P30 to P40 mice that were *in utero* electroporated at E14 with

hrGFP control or shSLK-hrGFP plasmids. We selected hrGFP-expressing neurons within cortical layers 2/3 for recording. First, we recorded spontaneous mEPSCs and mIPSCs (Fig. 4F). As predicted by the selective loss of inhibitory synapses in shSLK neurons, the mIPSC frequency was reduced by 43% (Fig. 4G, control [hrGFP] 10.0 ± 1.2 Hz vs shSLK-hrGFP 5.7 ± 1.1 Hz), whereas the mIPSC amplitude (Fig. 4H) was unchanged. In contrast, both the mEPSC frequency (Fig. 4I) and amplitude (Fig. 4J) were unchanged. To exclude that a change in the release probability of inhibitory synapses contributes to the reduction of the mIPSC frequency, we measured the PPR of stimulated IPSCs in hrGFP-expressing neurons (Fig. 4K). The PPR was calculated as the ratio of the amplitudes of two consecutively elicited IPSCs (IPSC2/IPSC1), and is an index of synaptic release probability. Paired-pulse depression of synaptically evoked IPSCs was unaltered in shSLK-hrGFP-expressing neurons compared with hrGFP control neurons (Fig. 4K). We also determined whether shSLK neurons exhibit changes in their active and passive properties. The input resistance was unchanged in shSLK neurons (Fig. 4L), although the cell capacitance was significantly reduced following SLK knockdown (Fig. 4M; control [hrGFP] 153.2 ± 10.2 pF vs shSLK-hrGFP 115.9 ± 13.2 pF), consistent with a smaller dendritic arbor (Figs. 1, 2). The active properties of SLK-deficient neurons were determined in current clamp by injecting 500 ms current steps of various magnitudes (Fig. 4N). There was no significant difference in the input-output responses for any current injection magnitude between hrGFP control and SLK-deficient neurons (Fig. 4N). AP properties were mostly unchanged in SLK knockdown neurons with only the peak depolarization rate being significantly reduced (Table 3). Collectively, the functional data suggest that the major functional phenotype of SLK-deficient excitatory neurons is a pronounced loss of functional inhibitory input.

SLK expression is lost in dysmorphic neurons of human epileptogenic malformations

Our data identify SLK to be essential for the development of a normal dendritic complexity and inhibitory synapse density in adulthood. These findings suggest that changes in SLK abundance might be associated with diseases that exhibit dysplastic neurons and an altered excitation-inhibition (E/I) balance, such as focal epileptogenic lesions. We therefore examined whether loss of SLK occurs in dysplastic neurons in FCDIIb and GGs. To this end, we performed coimmunolabeling of FCDIIb biopsies from epilepsy surgery of pharmacorefractory patients with antibodies against SLK and neuronal MAP-2. Quantification of SLK immunoreactivity revealed a robust loss of expression in dysmorphic FCDIIb neurons by 74% (nonlesioned control 216.2 ± 7.4 a.u. vs FCDIIb 55.4 ± 5.7 a.u.; Fig. 5A,B) compared with adjacent normal brain tissue. In dysmorphic neurons of GGs, SLK expression was reduced by 15% (control 677.8 ± 24.7 a.u. vs GG 573.5 ± 19.6 a.u.; Fig. 5C,D). SLK fluorescence colocalized with the neuronal protein MAP-2 but was undetectable in the vimentin-expressing glia cells (Fig. 5C). Dysmorphic neurons with fundamentally aberrant dendrite structure are the major cell type of the most frequent FCDIIb (with so-called balloon cells) (Blümcke et al., 2011). This feature is shared with GGs, the most common long-term epilepsy-associated tumors (Fig. 5E,F) (Thom et al., 2012). These data suggest a pathophysiological role for loss of SLK in dysmorphic, epileptogenic neurons.

←

dendrites: control vs shSLK: $p_{(t=5,015, df=114)} < 0.0001$; control vs SLK K63R: $p_{(t=5,145, df=114)} < 0.0001$; control vs shSLK + hSLK: $p_{(t=5,297, df=114)} < 0.0001$. E, No difference in dendrite length (in pixels) was observed in any tested condition. $n = 10$ control (hrGFP), $n = 9$ shSLK-hrGFP, $n = 12$ SLK K63R, and $n = 11$ shSLK-hrGFP + hSLK neurons. Experiment was repeated 3 times; repeated-measures two-way ANOVA (Interaction: $p_{(F=0.4064, df=6, 76)} = 0.8726$; Dendrite order: $p_{(F=43.59, df=2, 76)} < 0.0001$; Condition: $p_{(F=0.08865, df=3, 38)} = 0.9658$); Sidak's multiple-comparisons test, not significant, compared with control (in detail: Primary dendrites: control vs shSLK: $p_{(t=0.3519, df=114)} = 0.9793$; control vs SLK K63R: $p_{(t=0.2105, df=114)} = 0.9954$; control vs shSLK + hSLK: $p_{(t=0.6289, df=114)} = 0.8966$; Secondary dendrites: control vs shSLK: $p_{(t=0.2288, df=114)} = 0.9941$; control vs SLK K63R: $p_{(t=0.1861, df=114)} = 0.9968$; control vs shSLK + hSLK: $p_{(t=0.3104, df=114)} = 0.9856$; Higher-order dendrites: control vs shSLK: $p_{(t=0.506, df=114)} = 0.9424$; control vs SLK K63R: $p_{(t=0.6198, df=114)} = 0.9005$; control vs shSLK + hSLK: $p_{(t=1.113, df=114)} = 0.6079$).

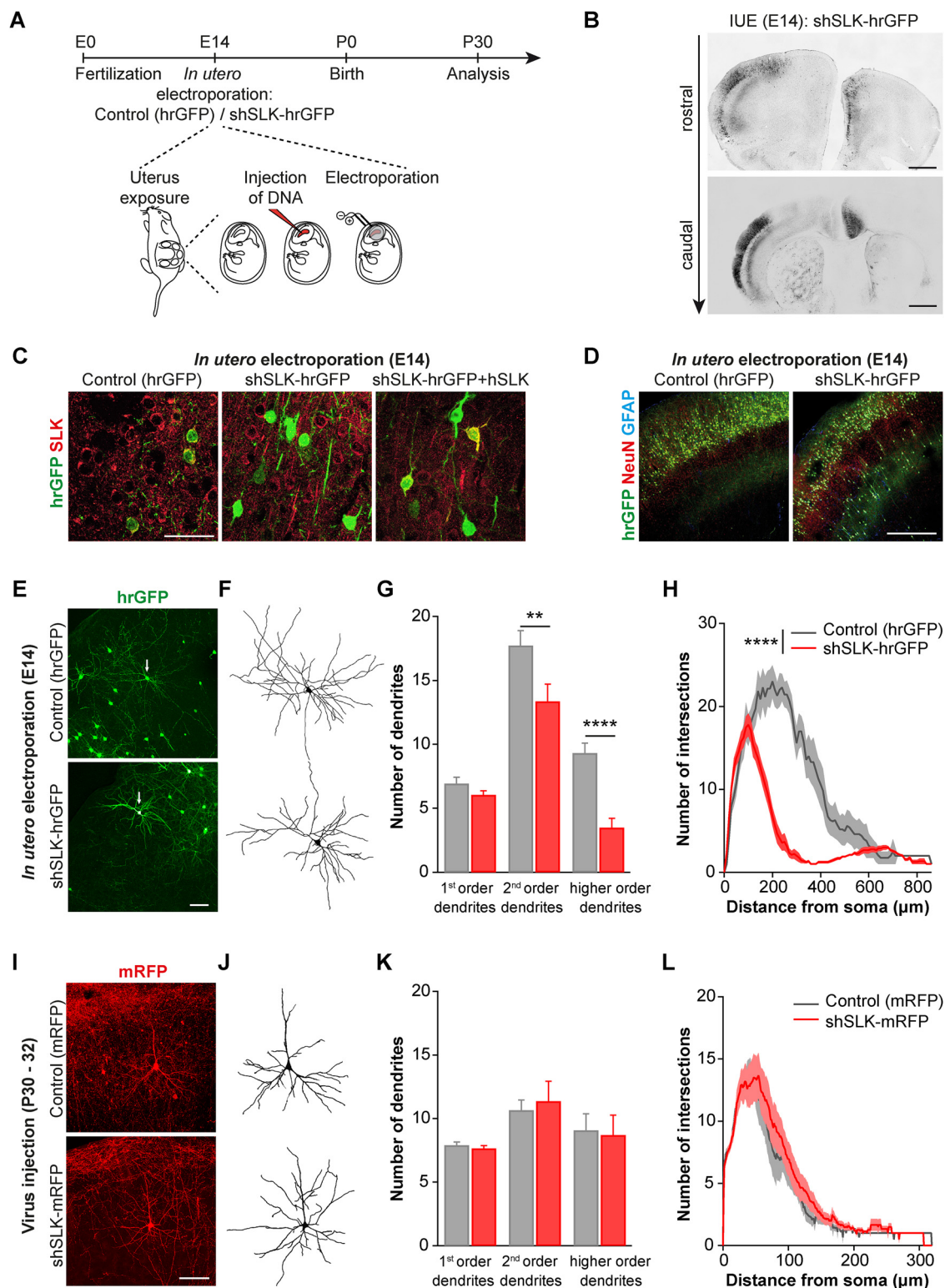


Figure 2. *In utero* knockdown of SLK leads to impaired dendritic branching in cortical neurons. **A**, Embryos of time pregnant CD1/C57BL/6-hybrid mice were *in utero* electroporated at E14 with hrGFP-labeled shSLK or control plasmids. **B**, Exemplary brain slices of a 30-d-old *in utero* electroporated mouse are depicted, illustrating the distribution of neurons expressing shSLK-hrGFP in cortical layers, from rostral to caudal. Scale bar, 1000 μm . **C**, Brain slices of mice *in utero* electroporated with hrGFP, shSLK-hrGFP, or shSLK-hrGFP combined with hSLK were stained with SLK antibodies. SLK staining is absent in shSLK neurons, whereas hrGFP and shSLK-hrGFP + hSLK plasmid-expressing neurons show moderate or strong SLK immunoreactivity. Scale bar, 50 μm . **D**, Immunohistochemical staining against NeuN and GFAP in hrGFP control- or shSLK-hrGFP-electroporated brain slices. Scale bar, 400 μm . **E**, Mice were *in utero* electroporated with hrGFP or shSLK-hrGFP, and dendrite outgrowth was analyzed at P30. Example images show control (hrGFP) or shSLK-hrGFP electroporated neurons that were chosen for reconstruction (white arrows). Scale bar, 100 μm . **F**, High-magnification images of reconstructed, multipolar, cortical neurons electroporated with either hrGFP-expressing control or shSLK-hrGFP plasmids. **G**, Quantification of the number of different order dendrites in hrGFP- or shSLK-hrGFP-electroporated brain slices shows robust reduction of distal dendrites in the absence of SLK. $N = 4$ and $N = 9$ mice from different litters with $n = 15$ control (hrGFP) and $n = 14$ shSLK-hrGFP neurons; repeated-measures two-way ANOVA (Interaction: $p_{(F=5.322; df=2, 54)} = 0.0078$; Dendrite order: $p_{(F=89.7; df=2, 54)} < 0.0001$; Condition: $p_{(F=18.28; df=1, 27)} = 0.0002$); Sidak's multiple-comparisons test, ** $p < 0.01$, **** $p < 0.0001$ (in detail: Primary dendrites: control vs shSLK:

Discussion

Dendrites are highly specialized neuronal compartments and the primary sites at which neurons receive, process, and integrate inputs from their multiple presynaptic partners. Here, we show for the first time, that the kinase SLK, a member of the evolutionarily conserved Ste20/Hippo kinase family, plays an important role in neuronal development. SLK-mediated phosphorylation critically regulates in a highly selective manner the formation of the distal dendritic tree during development and inhibitory synapse density. Loss of SLK leads to a less complex dendritic tree and impaired inhibition. Furthermore, SLK is lost in dysmorphic neurons of epileptogenic lesions, including FCDIIB and GGs, supporting a critical role of SLK during neuronal development.

SLK is required for the development of the distal dendritic tree but not for its maintenance

Our results show that the expression of SLK during development is selectively required for the formation of distal dendrites but not for their maintenance once they are formed. Our data further demonstrate that proper dendritic complexity depends on SLK kinase activity, since both the kinase-dead SLK K63R variant and shSLK expression resulted in similarly impaired dendritic architecture, and overexpression of SLK caused an increase in the number of higher-order dendrites. The most likely underlying mechanism is a modulation of cytoskeletal dynamics, which crucially underlies neurite growth and branching (Swiech et al., 2011; Sakakibara et al., 2013; Arthur et al., 2015; Yalgin et al., 2015) and which is regulated by SLK in non-neuronal cells. In this context, integrin signaling has been shown to be involved in the outgrowth and branching of dendrites, in part by impacting cytoskeletal dynamics (Moresco et al., 2005; Marrs et al., 2006), and SLK has been suggested to act downstream of integrin receptors (Wagner et al., 2008). Only few SLK substrates have been identified so far; however, among them are several cytoskeletal proteins, including RhoA (Guilluy et al., 2008), ezrin (Viswanatha et al., 2012; Machicoane et al., 2014), paxillin (Quizi et al., 2013), and the

←

$p_{(t=0.6894, df=81)} = 0.8693$; Secondary dendrites: control vs shSLK: $p_{(t=3.5, df=81)} = 0.0023$; Higher-order dendrites: control vs shSLK: $p_{(t=4.666, df=81)} < 0.0001$. **H**, Sholl analysis of single neurons also reveals a reduction in the complexity of the distal dendritic tree in SLK-deficient cortical neurons compared with hrGFP control neurons. $N = 4$ and $N = 6$ mice from different litters with $n = 7$ control (hrGFP) and $n = 9$ shSLK-hrGFP neurons; repeated-measures two-way ANOVA: Condition (control (hrGFP) vs shSLK-hrGFP): $****p < 0.0001$ (Interaction: $p_{(F=20.77, df=85, 1190)} < 0.0001$; Distance from soma: $p_{(F=58.53, df=85, 1190)} < 0.0001$; Condition: $p_{(F=60.67, df=1, 14)} < 0.0001$). **I**, Mice were intracortically injected with AAVs expressing mRFP or shSLK-mRFP, and dendrite outgrowth was analyzed 6 weeks later. Example images of control (mRFP) or shSLK-mRFP transduced neurons. Scale bar, 100 μm . **J**, Images of reconstructed, cortical neurons that were transduced with mRFP or shSLK-mRFP. **K**, Knocking down SLK in adult animals does not change the number of different order dendrites compared with control animals. $N = 4$ and $N = 6$ mice from different litters with $n = 29$ control (mRFP) and $n = 30$ shSLK-mRFP neurons; repeated-measures two-way ANOVA (Interaction: $p_{(F=0.1905, df=2, 16)} = 0.8284$; Dendrite order: $p_{(F=5.997, df=2, 16)} = 0.0114$; Condition: $p_{(F=0.0006349, df=1, 8)} = 0.9805$); Sidak's multiple-comparisons test, not significant (in detail: Primary dendrites: control vs shSLK: $p_{(t=0.1414, df=24)} = 0.9986$; Secondary dendrites: control vs shSLK: $p_{(t=0.4029, df=24)} = 0.9704$; Higher-order dendrites: control vs shSLK: $p_{(t=0.2024, df=24)} = 0.9960$). **L**, Sholl analysis after SLK knockdown at P30 shows no difference in the complexity of the dendritic arbor between control and shSLK-mRFP-expressing neurons. $N = 4$ and $N = 6$ mice from different litters with $n = 29$ control (mRFP) and $n = 30$ shSLK-mRFP neurons; repeated-measures two-way ANOVA: Condition (control (mRFP) vs shSLK-mRFP): not significant (Interaction: $p_{(F=0.4322, df=319, 2552)} > 0.9999$; Distance from soma: $p_{(F=75.37, df=319, 2552)} < 0.0001$; Condition: $p_{(F=0.3003, df=1, 8)} = 0.5986$).

p150^{Glued} dynactin subunit (Zhapparova et al., 2013). As components of the integrin signaling complex, ezrin and paxillin are involved in the regulation of the stability of actin fibers and both have been linked to the processes controlling dendrite morphogenesis (Myers and Gomez, 2011; Jin et al., 2018). RhoA acts as a negative regulator of dendritic arbor growth and dendrite number (H. Chen and Firestein, 2007), and its activity is inhibited by SLK, both by direct phosphorylation of RhoA and indirectly by phosphorylating ezrin that then inhibits RhoA (Guilluy et al., 2008; Al-Zahrani et al., 2020), suggesting that one pathway by which SLK controls dendritic tiling is via RhoA. This shows that multiple candidate downstream mechanisms are already known that could affect neuronal processes. However, studies of SLK function have revealed that the kinase triggers different downstream cascades in distinct non-neuronal cell types. It will therefore be important to resolve which signaling cascades are regulated by SLK in neurons and how they differ between development and adulthood.

Functionally, the selective impact of SLK loss on the formation of distal dendrites is intriguing because the length and structure of the dendritic arbor profoundly influence signal integration and thereby neuronal network function (Katz et al., 2009; Warren et al., 2012; Menon et al., 2013). Future studies will have to resolve how this specific deficit impacts the properties of the connected neuronal networks.

SLK selectively regulates inhibitory synapse density in the period of synapse stabilization

One intriguing finding of our study is the selective impact of SLK deficiency on the density of inhibitory synapses during development. Inhibitory synapses initially develop normally, but their density is significantly reduced after P15. Therefore, SLK is not required for the initial formation of inhibitory synapses but rather for the stabilization of already formed postsynaptic structures. After their initial establishment, inhibitory synapses need to be actively maintained to ensure their proper functionality (Sfakianos et al., 2007; Lin and Koleske, 2010). This process involves the dynamic interaction of the inhibitory synapse-specific protein scaffold with cytoskeletal filaments and cytoskeleton-interacting proteins and is regulated by phosphorylation (Kirsch and Betz, 1995; Yamauchi, 2002; Bausen et al., 2006; Okabe, 2007; Tyagarajan et al., 2011; Tyagarajan and Fritschy, 2014; Choi and Ko, 2015).

In contrast to excitatory synapses, both the actin and the microtubule cytoskeleton are thought to participate in stabilizing the inhibitory postsynaptic scaffolding complex (Harvey et al., 2004; Bausen et al., 2006; Papadopoulos et al., 2008). This difference might explain the selective role of SLK in stabilizing the inhibitory postsynapse. As mentioned above, SLK has been reported to regulate actin and microtubule dynamics downstream of integrin signaling. It was shown that integrins control the level of gephyrin at inhibitory synapses (Charrier et al., 2010), suggesting a role for this complex and thereby maybe also for SLK in the control of inhibitory synapse stability.

This selective loss of inhibitory synapses might have pathologic consequences as it was recently demonstrated that loss of local inhibition caused by a destabilization of already formed inhibitory synapses leads to a pathologic neuronal network manifesting with complex symptoms, including impaired anxiety, fear memory, and social interaction behavior (Papadopoulos et al., 2008; Lin and Koleske, 2010; Liang et al., 2015).

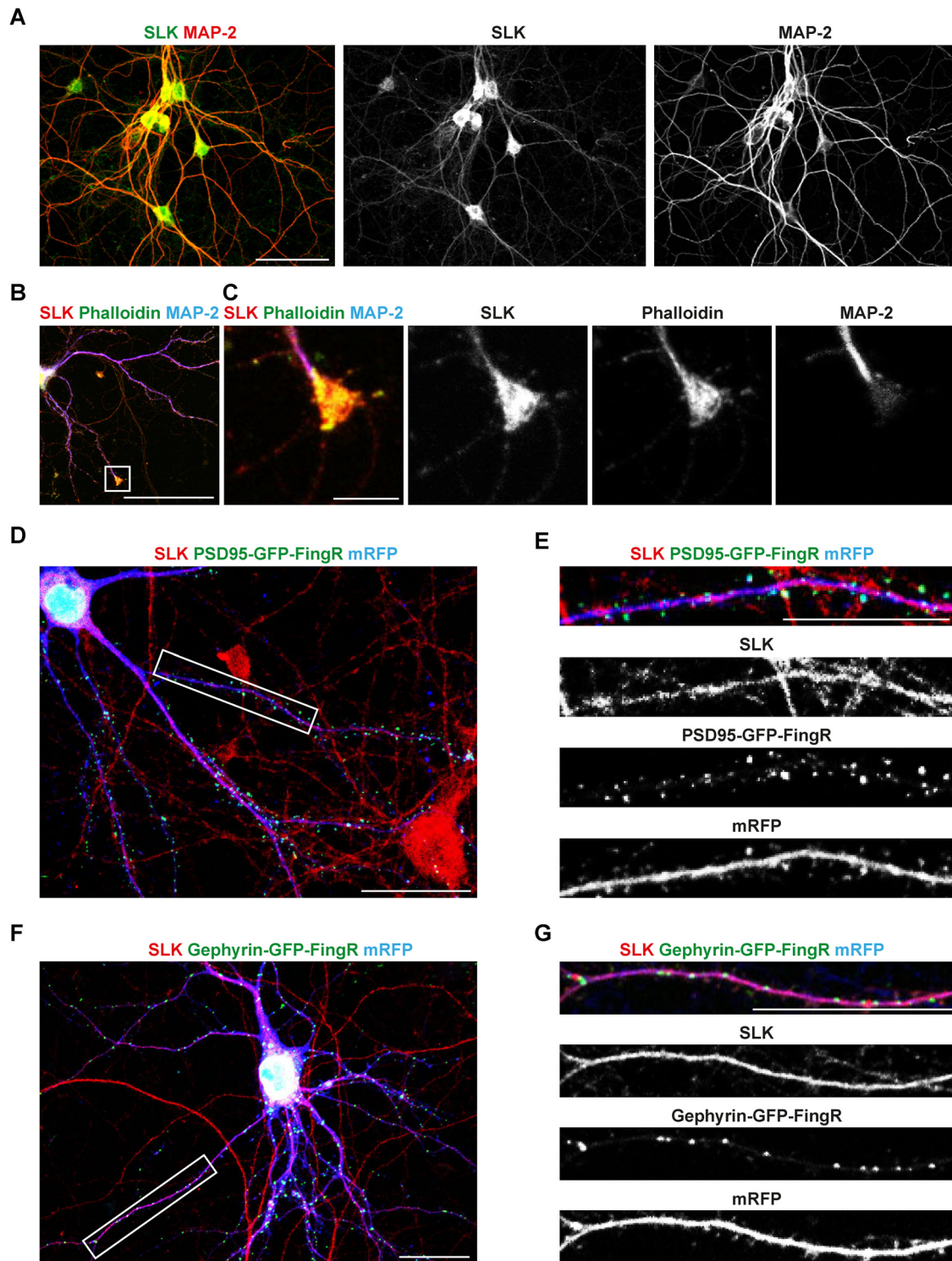


Figure 3. Strong coexpression with gephyrin localizes SLK to inhibitory postsynapses. **A**, Cultured cortical neurons were fixed and stained against MAP-2 or SLK at DIV14. Scale bar, 50 μ m. **B**, Cultured cortical neurons were transfected at DIV4 with mRFP, stained with SLK, MAP-2 antibodies, and phalloidin, and analyzed at DIV14. Scale bar, 50 μ m. **C**, Close-up of the growth cone shows colocalization of SLK and F-actin. Scale bar, 6 μ m. **D**, Cultured cortical neurons were transfected at DIV4 with mRFP and PSD95-GFP-FingRs, stained with SLK antibodies at DIV21, and overlap of PSD95⁺ punctae and SLK was assessed. Scale bar, 25 μ m. **E**, Only little spatial overlap between SLK and PSD95-GFP-FingRs can be observed. Scale bar, 25 μ m. **F**, Cultured cortical neurons were transfected at DIV4 with mRFP and gephyrin-GFP-FingRs and stained with SLK antibodies at DIV21. Scale bar, 25 μ m. **G**, Gephyrin-GFP overlaps spatially with SLK staining. Scale bar, 25 μ m.

SLK loss in dysmorphic neurons of human developmental brain lesions as pathomechanism underlying epileptogenic network formation

Impaired inhibitory neuronal signaling or altered E/I balance may be a common phenomenon across the spectrum of

disorders associated with epilepsy. In acquired temporal lobe epilepsy models, multiple changes in the GABAergic system have been described. In Alzheimer's disease models, loss of a sodium channel isoform (Nav1.1) expressed mainly in interneurons seems to cause hyperexcitability (Palop et al., 2007; Verret et al.,

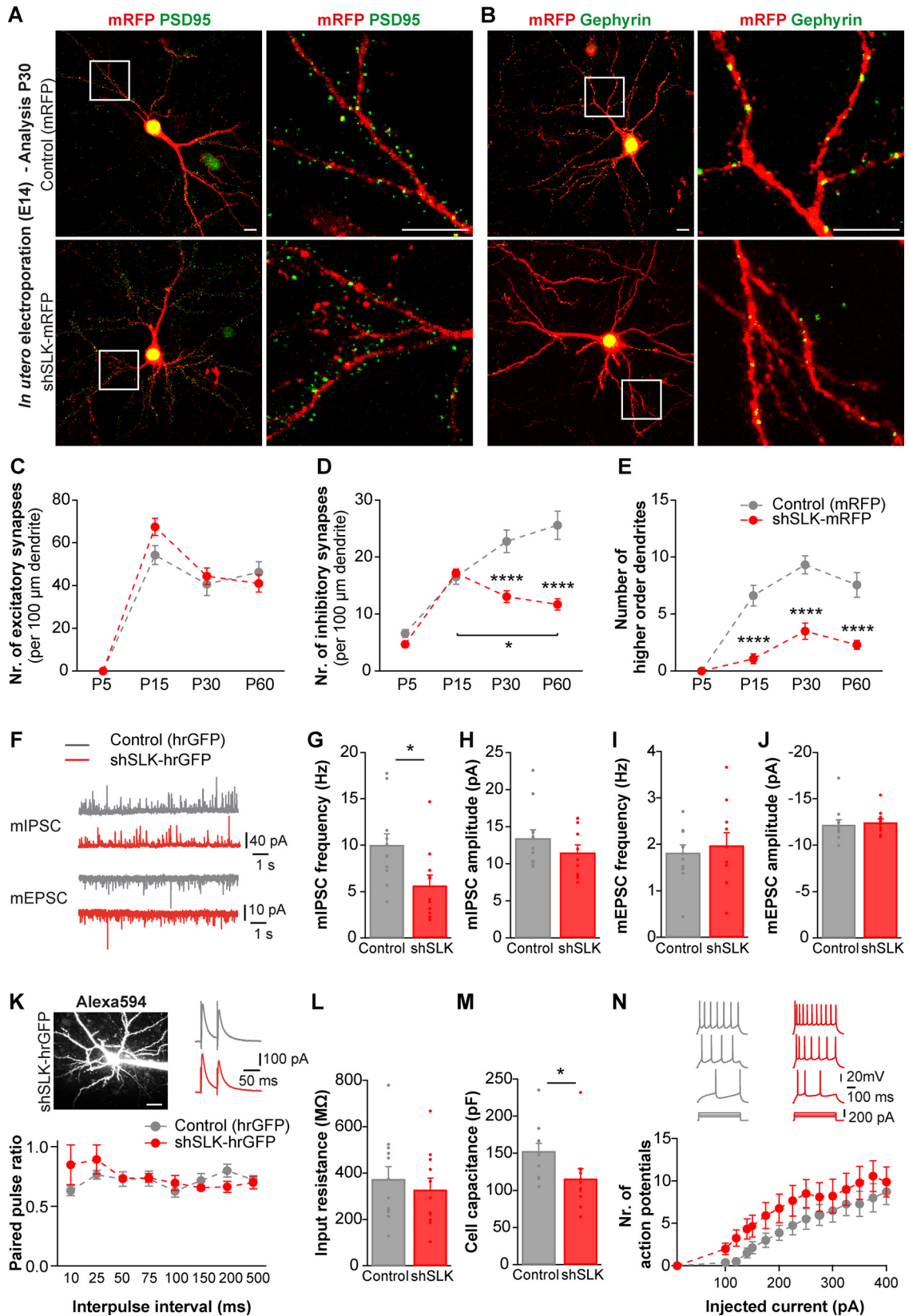


Figure 4. shRNA-mediated SLK knockdown reduces inhibitory postsynapse density and mIPSC frequency. **A**, Exemplary neurons of 30-d-old mice *in utero* co-electroporated at E14 with mRFP (control) or shSLK-mRFP together with PSD95-GFP-FingRs. White squares represent areas of higher magnification seen in the right panel, depicting first- and second-order dendrites. Scale bar, 10 μm . **B**, Exemplary images of cortical neurons electroporated with gephyrin-GFP-FingRs together with mRFP or shSLK-mRFP. Right, Area within the white square at higher magnification. Scale bar, 10 μm . **C**, PSD95⁺ postsynapse density is unchanged at P5, P15, P30, or P60 in shSLK-mRFP-expressing neurons compared with control. Excitatory synapse quantification: in total P5: $N = 4$ and $N = 4$ mice from different litters with $n = 9$ control (mRFP) and $n = 9$ shSLK-mRFP neurons; P15: $N = 4$ and $N = 4$ mice from different litters with $n = 7$ control (mRFP) and $n = 7$ shSLK-mRFP neurons; P30: $N = 5$ and $N = 7$ mice from different litters with $n = 10$ control (mRFP) and $n = 14$ shSLK-mRFP neurons; P60: $N = 4$ and $N = 4$ mice from different litters

2012). In autism spectrum disorders, E/I imbalance seems to occur mainly via loss of excitatory synapses (Anderson et al., 2012; Schmeisser et al., 2012). In contrast, in a mouse model of tuberous sclerosis, E/I imbalance is increased because of a

←

with $n = 9$ control (mRFP) and $n = 7$ shSLK-mRFP neurons; two-way ANOVA (Interaction: $p_{(F=1.649, df=3, 64)} = 0.1868$; Time point: $p_{(F=81.85, df=3, 64)} < 0.0001$; Condition: $p_{(F=1.429, df=1, 64)} = 0.2363$); Tukey's multiple-comparisons test, not significant (in detail: P5: control vs shSLK: $p_{(q=0, df=64)} > 0.9999$; P15: control vs shSLK: $p_{(q=2.906, df=64)} = 0.4546$; P30: control vs shSLK: $p_{(q=1.669, df=64)} = 0.9346$; P60: control vs shSLK: $p_{(q=1.213, df=64)} = 0.9887$). **D**, Inhibitory synapse density is quantified for mice at P5, P15, P30, and P60 and shows no difference at P5 and P15 but a significant reduction at P30 and P60 when electroporating shSLK-mRFP compared with control mRFP. Inhibitory synapse quantification: in total P5: $N = 5$ and $N = 5$ mice from different litters with $n = 19$ control (mRFP) and $n = 21$ shSLK-mRFP neurons; P15: $N = 6$ and $N = 8$ mice from different litters with $n = 15$ control (mRFP) and $n = 24$ shSLK-mRFP neurons; P30: $N = 6$ and $N = 6$ mice from different litters with $n = 10$ control (mRFP) and $n = 11$ shSLK-mRFP neurons; P60: $N = 4$ and $N = 4$ mice from different litters with $n = 10$ control (mRFP) and $n = 10$ shSLK-mRFP neurons; two-way ANOVA (Interaction: $p_{(F=16.65, df=3, 112)} < 0.0001$; Time point: $p_{(F=70.74, df=3, 112)} < 0.0001$; Condition: $p_{(F=57.16, df=1, 112)} < 0.0001$); Tukey's multiple-comparisons test, $*p < 0.05$, $***p < 0.0001$ compared with mRFP control, unless indicated otherwise (in detail: P5: control vs shSLK: $p_{(q=2.001, df=112)} = 0.8485$; P15: control vs shSLK: $p_{(q=0.6873, df=112)} = 0.9997$; P30: control vs shSLK: $p_{(q=7.411, df=112)} < 0.0001$; P60: control vs shSLK: $p_{(q=10.36, df=112)} < 0.0001$; shSLK: P15 vs P60: $p_{(q=4.875, df=112)} = 0.0176$). **E**, The number of higher-order dendrites is reduced in shSLK-expressing cortical neurons starting from P15 persisting to P60. Dendrite quantification: in total P5: $N = 4$ and $N = 5$ mice from different litters with $n = 5$ control (mRFP) and $n = 10$ shSLK-mRFP neurons; P15: $N = 4$ and $N = 4$ mice from different litters with $n = 8$ control (mRFP) and $n = 12$ shSLK-mRFP neurons; P30: $N = 4$ and $N = 9$ mice from different litters with $n = 15$ control (mRFP) and $n = 14$ shSLK-mRFP neurons; P60: $N = 4$ and $N = 5$ mice from different litters with $n = 9$ control (mRFP) and $n = 10$ shSLK-mRFP neurons; two-way ANOVA (Interaction: $p_{(F=5.598, df=3, 75)} = 0.0016$; Time point: $p_{(F=24.68, df=3, 75)} < 0.0001$; Condition: $p_{(F=61.72, df=1, 75)} < 0.0001$); Sidak's multiple-comparisons test, $***p < 0.0001$ compared with mRFP control (in detail: P5: control vs shSLK: $p_{(t=0, df=75)} > 0.9999$; P15: control vs shSLK: $p_{(t=5.311, df=75)} < 0.0001$; P30: control vs shSLK: $p_{(t=6.867, df=75)} < 0.0001$; P60: control vs shSLK: $p_{(t=5.004, df=75)} < 0.0001$). **F**, Example traces of voltage-clamp recordings of mIPSCs and mEPSCs from hrGFP control and shSLK-hrGFP-expressing neurons. **G, H**, Patch-clamp recordings of mIPSCs (holding potential 0 mV) showed a decrease in mIPSC frequency in shSLK-hrGFP electroporated cells, whereas the mIPSC amplitude was not changed. Unpaired two-tailed t test: $*p < 0.05$ (**G**, $p_{(t=2.639, df=21)} = 0.0154$; **H**, $p_{(t=1.241, df=21)} = 0.2281$). **I, J**, mEPSC frequency (holding potential -60 mV) and amplitude were not different in shSLK-hrGFP-expressing neurons compared with hrGFP control. Unpaired two-tailed t test: not significant (**I**, $p_{(t=0.5102, df=21)} = 0.6153$; **J**, $p_{(t=0.4026, df=21)} = 0.6913$). **K**, Example image of an shSLK-expressing neuron that was filled with Alexa-594. Scale bar, 20 μ m. The PPR of two electrically elicited IPSCs remained unchanged in control (hrGFP) and shSLK-hrGFP cells. $n = 6$ control (hrGFP) and $n = 6$ shSLK-hrGFP neurons; two-way ANOVA (Interaction: $p_{(F=1.225, df=7, 75)} = 0.3000$; Interpulse interval: $p_{(F=0.8838, df=7, 75)} = 0.5235$; Condition: $p_{(F=0.4102, df=1, 75)} = 0.5238$); Sidak's multiple-comparisons test: not significant (in detail: 10 ms: $p_{(t=2.233, df=75)} = 0.2067$; 25 ms: $p_{(t=1.327, df=75)} = 0.8119$; 50 ms: $p_{(t=0.0808, df=75)} > 0.9999$; 75 ms: $p_{(t=0.07856, df=75)} > 0.9999$; 100 ms: $p_{(t=0.3747, df=75)} > 0.9999$; 150 ms: $p_{(t=0.5876, df=75)} = 0.9986$; 200 ms: $p_{(t=1.345, df=75)} = 0.8011$; 500 ms: $p_{(t=0.2252, df=75)} > 0.9999$). **L, M**, Input resistance was comparable in both groups, whereas the cell capacitance was significantly reduced in the shSLK-hrGFP group. Unpaired two-tailed t test: $*p < 0.05$ (**L**, $p_{(t=0.6224, df=21)} = 0.5404$; **M**, $p_{(t=2.262, df=21)} = 0.0344$). **N**, Number of APs elicited by 500 ms depolarizing current steps. Input-output responses did not differ for any current injection magnitude between control (hrGFP) and shSLK-hrGFP-expressing neurons. $n = 8$ control (hrGFP) and $n = 12$ shSLK-hrGFP neurons; two-way ANOVA (Interaction: $p_{(F=0.1827, df=14, 249)} = 0.9996$; Injected current: $p_{(F=9.08, df=14, 249)} < 0.0001$; Condition: $p_{(F=18.51, df=1, 249)} < 0.0001$); Sidak's multiple-comparisons test, not significant (in detail: 10 pA: $p_{(t=0, df=249)} > 0.9999$; 100 pA: $p_{(t=0.8432, df=249)} = 0.9995$; 120 pA: $p_{(t=1.427, df=249)} = 0.9198$; 140 pA: $p_{(t=1.47, df=249)} = 0.9008$; 150 pA: $p_{(t=1.319, df=249)} = 0.9564$; 175 pA: $p_{(t=1.513, df=249)} = 0.8792$; 200 pA: $p_{(t=1.492, df=249)} = 0.8903$; 225 pA: $p_{(t=1.513, df=249)} = 0.8792$; 250 pA: $p_{(t=1.557, df=249)} = 0.8551$; 275 pA: $p_{(t=1.049, df=249)} = 0.9948$; 300 pA: $p_{(t=0.8394, df=249)} = 0.9996$; 325 pA: $p_{(t=0.853, df=249)} = 0.9995$; 350 pA: $p_{(t=1.171, df=249)} = 0.9845$; 375 pA: $p_{(t=1.201, df=249)} = 0.9805$; 400 pA: $p_{(t=0.5312, df=249)} > 0.9999$). **G–J, L, M**, $N = 3$ and $N = 5$ mice with $n = 12$ control (hrGFP) and $n = 11$ shSLK-hrGFP neurons.

Table 3. AP properties^a

AP properties	Control (hrGFP) ($n = 8$)	shSLK-hrGFP ($n = 12$)
Peak potential	35.1 \pm 1.7	32.3 \pm 1.8
Peak depolarization rate (V/s)	366 \pm 25	319 \pm 20**
Peak repolarization rate (V/s)	-70.3 \pm 2.7	-58.4 \pm 2.8
Threshold (mV)	-50.3 \pm 1.0	-46.5 \pm 1.6
Duration at half-amplitude (ms)	1.1 \pm 0.04	1.25 \pm 0.06
Fast afterhyperpolarization amplitude (mV)	5.9 \pm 1.1	6.1 \pm 1.6

^aAPs were recorded from cells expressing control (hrGFP) or shSLK (shSLK-hrGFP) encoding plasmids that were introduced by IUE at E14. $n = 8$ control (hrGFP) and $n = 12$ shSLK-hrGFP neurons; two-way ANOVA (interaction: $p_{(F=2.497, df=5, 108)} = 0.0351$; AP properties: $p_{(F=516, df=5, 108)} < 0.0001$; condition: $p_{(F=1.086, df=1, 108)} = 0.2997$); Sidak's multiple-comparisons test, $***p < 0.01$, for comparison between indicated value and respective control value (in detail: peak potential: $p_{(t=0.2118, df=108)} > 0.9999$; peak depolarization rate: $p_{(t=3.555, df=108)} = 0.0034$; peak repolarization rate: $p_{(t=0.9, df=108)} = 0.9376$; threshold: $p_{(t=0.2874, df=108)} = 0.9999$; duration at half amplitude: $p_{(t=0.01134, df=108)} > 0.9999$; fast afterhyperpolarization amplitude: $p_{(t=0.01513, df=108)} > 0.9999$).

reduction in inhibitory synapse function (Bateup et al., 2013). Our discovery of an SLK-mediated E/I imbalance provides an intriguing new aspect to this range of mechanisms. Furthermore, novel gene mutations of SLK found in families with intellectual disability point to the importance of SLK's role for proper CNS development and the substantial potential of aberrant neuronal network function in the case of SLK impairment (Anazi et al., 2017).

With respect to hyperexcitable brain malformations, several recent studies have significantly advanced our understanding of the pathogenic events that initiate the formation of FCDs and GGs (Koelsche et al., 2013; Koh et al., 2018; Baldassari et al., 2019). Less is known on how the characteristic morphologic and functional neuronal phenotypes of FCDII and GGs develop. Several aspects of our mouse model and human data suggest loss of SLK as a significant pathomechanism for the emergence of dysmorphic neurons in focal lesions. First, reduced expression of SLK is present in both FCDIIb and GGs, despite their substantially different molecular-genetic backgrounds (Koelsche et al., 2013; Lim et al., 2015). Second, although many genes are differentially expressed in dysmorphic lesions, knockdown of just SLK had a profound and selective effect on neuronal, particularly dendritic, morphology and function. The resulting E/I imbalance of a relatively restricted, focal ensemble of neurons could contribute to the episodic generation of epileptiform activity. Of note, intellectual disability is a frequent comorbidity in FCD patients, and SLK has been recently reported as a potential intellectual disability risk gene (Anazi et al., 2017). Decreased inhibition is a key feature of many focal cortical malformation models (Calcagnotto et al., 2005; André et al., 2010; Talos et al., 2012), and our data suggest that reduced SLK levels in dysplastic neurons might contribute to the development of these lesions in humans, despite the large spectrum of dendritic impairment in neuronal elements of FCDs, which comprise both hyper- and hypo-arborized dendrites (Rossini et al., 2021). It should further be noted that, in FCDs, a significant reduction in IPSC frequency and a potentially compensatory decrease in transporter-mediated GABA reuptake function (Calcagnotto et al., 2005) but also a higher frequency of spontaneous IPSCs presumably because of altered GABA_A receptor subunit composition have been reported (André et al., 2010). The complexity of inhibitory signal transmission of FCDs will require further network-based analyses in the future for which SLK knockdown appears as a suitable model. A further intriguing observation in our experiments was that SLK influences rather the maintenance than the initial development of inhibitory synapses, which may be in line with the clinical notion that most FCDIIb and GG patients do not develop epilepsy before early childhood (Sisodiya et al., 2009).

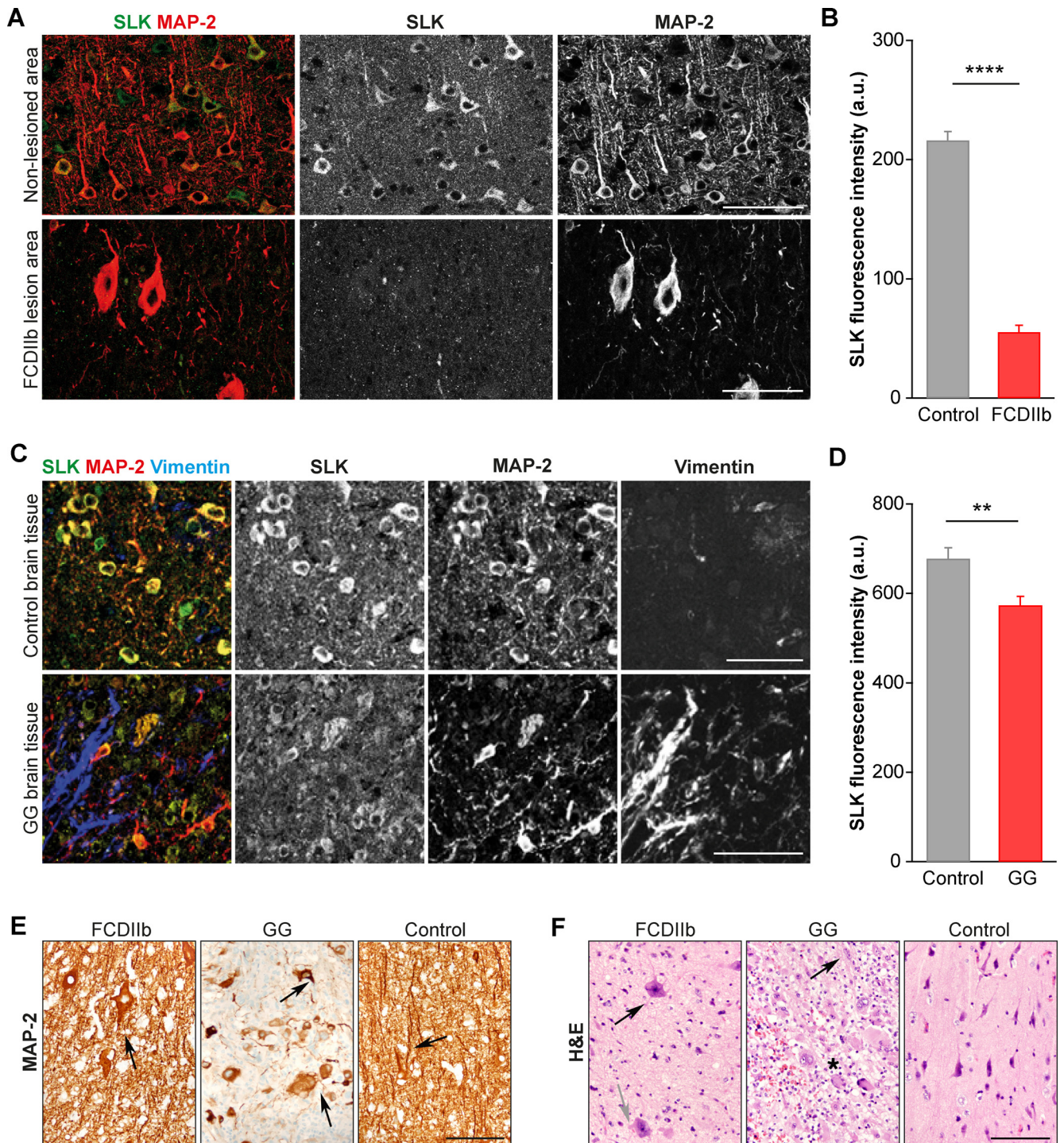


Figure 5. Dysmorphic neurons with aberrant dendritic architecture show loss of SLK immunoreactivity in human epileptogenic developmental lesions. **A**, The expression of SLK was compared between normal human brain tissue/nonlesioned control tissue and the adjacent dysmorphic lesion. Coimmunohistochemistry of FCDIIb specimens with antibodies against SLK and MAP-2 reveals SLK-expressing neurons in control areas, whereas SLK immunoreactivity in large dysmorphic neurons in the lesioned cortex is almost absent. Scale bar, 100 μ m. **B**, Quantification of SLK fluorescence intensity shows low values for dysmorphic neurons within the FCDIIb-lesioned area compared with neurons in the normal-appearing columnar cortex. $N = 10$ different patients with a total of $n = 269$ control and $n = 94$ dysmorphic neurons. Unpaired two-tailed t test: **** $p < 0.0001$ ($p_{(t=12.32, df=361)} < 0.0001$). **C**, In GGs (i.e., benign human brain tumors harboring dysmorphic neurons), coimmunohistochemistry with antibodies against SLK, MAP-2, and vimentin revealed strong expression of SLK in MAP-2-expressing (i.e., neuronal elements) but not in vimentin-positive astroglial cells in control brain tissue. Scale bar, 100 μ m. **D**, The expression of SLK is substantially reduced in dysmorphic neuronal (i.e., MAP-2 positive elements) in GG. $N = 8$ different patients with $n = 613$ control cells and $n = 466$ cells within the GG. Unpaired two-tailed t test: ** $p < 0.01$ ($p_{(t=3.15, df=1077)} = 0.0017$). **E**, Human specimens of FCDIIb and GGs were stained with antibodies against MAP-2. Highly enlarged dysmorphic neurons in an FCDIIb; note the aberrantly thick and short neurites (FCDIIb, black arrow). Substantially pathologic architecture of neurites in GG; note the shortened processes of aberrant and strongly varying diameter (GG, black arrows). Delicate process pattern in normal cerebral cortex structures (control, black arrow). Scale bar, 100 μ m. **F**, H&E staining of human specimens of FCDIIb and GGs. Very large, irregularly oriented dysmorphic neurons with aberrantly thin (FCDIIb, gray arrow) or particularly strong processes (FCDIIb, black arrow) without organoid organization in very low cellular matrix indicating a dysmorphic (FCDIIb) rather than neoplastic process. Clusters of sometimes even binucleated (GG, black arrow) dysmorphic neurons (GG, asterisk) in a cellular matrix of neoplastic astroglia in GG. Normal cerebral cortex structures, which have a clear organoid organization (control). Scale bar, 100 μ m.

In conclusion, our data attribute to SLK a critical and highly selective role in the regulation of dendritic complexity during development and of inhibitory synapse stabilization. Our results also suggest that SLK contributes to morpho-functional abnormalities in dysmorphic neurons of highly epileptogenic brain lesions.

References

- Al-Zahrani KN, Abou-Hamad J, Cook DP, Pryce BR, Hodgins JJ, Labrèche C, Robineau-Charette P, de Souza CT, Bell JC, Auer RC, Ardolino M, Vanderhyden BC, Sabourin LA (2020) Loss of the Ste20-like kinase induces a basal/stem-like phenotype in HER2-positive breast cancers. *Oncogene* 39:4592–4602.
- Al-Zahrani KN, Baron KD, Sabourin LA (2013) Ste20-like kinase SLK, at the crossroads: a matter of life and death. *Cell Adh Migr* 7:1–10.
- Al-Zahrani KN, Sekhon P, Tessier DR, Yockell-Lelievre J, Pryce BR, Baron KD, Howe GA, Sriram RK, Daniel K, McKay M, Lo V, Quizi J, Addison CL, Gruslin A, Sabourin LA (2014) Essential role for the SLK protein kinase in embryogenesis and placental tissue development. *Dev Dyn* 243:640–651.
- Alvarez-Baron E, Michel K, Mittelstaedt T, Opitz T, Schmitz F, Beck H, Dietrich D, Becker AJ, Schoch S (2013) RIM3 γ and RIM4 γ are key regulators of neuronal arborization. *J Neurosci* 33:824–839.
- Anazi S, Maddirevula S, Salpietro V, Asi YT, Alsahli S, Alhashem A, Shamseldin HE, AlZahrani F, Patel N, Ibrahim N, Abdulwahab FM, Hashem M, Alhashmi N, Al Murshedi F, Al Kindy A, Alshaer A, Rumayyan A, Al Tala S, Kurdi W, Alsaman A, et al. (2017) Expanding the genetic heterogeneity of intellectual disability. *Hum Genet* 136:1419–1429.
- Anderson GR, Galfin T, Xu W, Aoto J, Malenka RC, Südhof TC (2012) Candidate autism gene screen identifies critical role for cell-adhesion molecule CASPR2 in dendritic arborization and spine development. *Proc Natl Acad Sci USA* 109:18120–18125.
- André VM, Cepeda C, Vinters HV, Huynh M, Mathern GW, Levine MS (2010) Interneurons, GABA currents, and subunit composition of the GABA A receptor in type I and type II cortical dysplasia. *Epilepsia* 51 Suppl 3:166–170.
- Arikath J, Reichardt LF (2008) Cadherins and catenins at synapses: roles in synaptogenesis and synaptic plasticity. *Trends Neurosci* 31:487–494.
- Arthur AL, Yang SZ, Abellana AM, Wildonger J (2015) Dendrite arborization requires the dynein cofactor NudE. *J Cell Sci* 128:2191–2201.
- Baldassari S, Ribierre T, Marsan E, Adle-Biassette H, Ferrand-Sorbets S, Bulteau C, Dorison N, Fohlen M, Polivka M, Weckhuysen S, Dorfmüller G, Chipaux M, Baulac S (2019) Dissecting the genetic basis of focal cortical dysplasia: a large cohort study. *Acta Neuropathol* 138:885–900.
- Bateup HS, Johnson CA, Deneffrio CL, Saulnier JL, Kornacker K, Sabatini BL (2013) Excitatory/inhibitory synaptic imbalance leads to hippocampal hyperexcitability in mouse models of tuberous sclerosis. *Neuron* 78:510–522.
- Bausen M, Fuhrmann JC, Betz H, O'Sullivan GA (2006) The state of the actin cytoskeleton determines its association with gephyrin: role of ena/VASP family members. *Mol Cell Neurosci* 31:376–386.
- Blümcke I, Thom M, Aronica E, Armstrong DD, Vinters HV, Palmieri A, Jacques TS, Avanzini G, Barkovich AJ, Battaglia G, Becker A, Cepeda C, Cendes F, Colombo N, Crino P, Cross JH, Delalande O, Dubeau F, Duncan J, Guerrini R, et al. (2011) The clinicopathologic spectrum of focal cortical dysplasias: a consensus classification proposed by an ad hoc Task Force of the ILAE Diagnostic Methods Commission. *Epilepsia* 52:158–174.
- Calcagnotto ME, Paredes MF, Tihan T, Barbaro NM, Baraban SC (2005) Dysfunction of synaptic inhibition in epilepsy associated with focal cortical dysplasia. *J Neurosci* 25:9649–9657.
- Charrier C, MacHado P, Tweedie-Cullen RY, Rutishauser D, Mansuy IM, Triller A (2010) A crosstalk between $\beta 1$ and $\beta 3$ integrins controls glycine receptor and gephyrin trafficking at synapses. *Nat Neurosci* 13:1388–1395.
- Chen H, Firestein BL (2007) RhoA regulates dendrite branching in hippocampal neurons by decreasing cypin protein levels. *J Neurosci* 27:8378–8386.
- Chen X, Shibata AC, Hendi A, Kurashina M, Fortes E, Weilingner NL, MacVicar BA, Murakoshi H, Mizumoto K (2018) Rap2 and TNIK control plexin-dependent tiled synaptic innervation in *C. elegans*. *Elife* 7:e38801.
- Choi H, Ko J (2015) Gephyrin: a central GABAergic synapse organizer. *Exp Mol Med* 47:e158.
- Emoto K, Parrish JZ, Jan LY, Jan YN (2006) The tumour suppressor Hippo acts with the NDR kinases in dendritic tiling and maintenance. *Nature* 443:210–213.
- Ferrante M, Migliore M, Ascoli GA (2013) Functional impact of dendritic branch-point morphology. *J Neurosci* 33:2156–2165.
- Gross G, Junge J, Mora R, Kwon HB, Olson CA, Takahashi T, Liman E, Ellis-Davies GR, McGee A, Sabatini B, Roberts R, Arnold D (2013) Recombinant probes for visualizing endogenous synaptic proteins in living neurons. *Neuron* 78:971–985.
- Grote A, Robens BK, Blümcke I, Becker AJ, Schoch S, Gembé E (2016) LRP12 silencing during brain development results in cortical dyslamination and seizure sensitization. *Neurobiol Dis* 86:170–176.
- Guilluy C, Rolli-Derkinderen M, Loufrani L, Bourgué A, Henrien D, Sabourin L, Loirand G, Pacaud P (2008) Ste20-related kinase SLK phosphorylates Ser188 of RhoA to induce vasodilation in response to angiotensin II Type 2 receptor activation. *Circ Res* 102:1265–1274.
- Harvey K, Duguid IC, Alldred MJ, Beatty SE, Ward H, Keep NH, Lingenfelter SE, Pearce BR, Lundgren J, Owen MJ, Smart TG, Lüscher B, Rees MI, Harvey RJ (2004) The GDP-GTP exchange factor collybistin: an essential determinant of neuronal gephyrin clustering. *J Neurosci* 24:5816–5826.
- Hussain NK, Hsin H, Haganir RL, Sheng M (2010) MINK and TNIK differentially act on Rap2-mediated signal transduction to regulate neuronal structure and AMPA receptor function. *J Neurosci* 30:14786–14794.
- Jan YN, Jan LY (2010) Branching out: mechanisms of dendritic arborization. *Nat Rev Neurosci* 11:316–328.
- Jin EJ, Ko HR, Hwang I, Kim BS, Choi JY, Park KW, Cho SW, Ahn JY (2018) Akt regulates neurite growth by phosphorylation-dependent inhibition of radixin proteasomal degradation. *Sci Rep* 8:2557.
- Katz Y, Menon V, Nicholson DA, Geinisman Y, Kath WL, Spruston N (2009) Synapse distribution suggests a two-stage model of dendritic integration in CA1 pyramidal neurons. *Neuron* 63:171–177.
- Kerrisk ME, Greer CA, Koleske AJ (2013) Integrin $\alpha 3$ is required for late postnatal stability of dendrite arbors, dendritic spines and synapses, and mouse behavior. *J Neurosci* 33:6742–6752.
- Kirsch J, Betz H (1995) The postsynaptic localization of the glycine receptor-associated protein gephyrin is regulated by the cytoskeleton. *J Neurosci* 15:4148–4156.
- Koelsche C, Wöhrer A, Jeibmann A, Schittenhelm J, Schindler G, Preusser M, Lasitschka F, Von Deimling A, Capper D (2013) Mutant BRAF V600E protein in ganglioglioma is predominantly expressed by neuronal tumor cells. *Acta Neuropathol* 125:891–900.
- Koh HY, Kim SH, Jang J, Kim H, Han S, Lim JS, Son G, Choi J, Park BO, Do Heo W, Han J, Lee HJ, Lee D, Kang HC, Shong M, Paik SB, Kim DS, Lee JH (2018) BRAF somatic mutation contributes to intrinsic epileptogenicity in pediatric brain tumors. *Nat Med* 24:1662–1668.
- Köhrmann M, Haubensak W, Hemraj J, Kaether C, Leßmann VJ, Kiebler MA (1999) Fast, convenient, and effective method to transiently transfect primary hippocampal neurons. *J Neurosci Res* 58:831–835.
- Liang J, Xu W, Hsu YT, Yee AX, Chen L, Südhof TC (2015) Conditional neuroigin-2 knockout in adult medial prefrontal cortex links chronic changes in synaptic inhibition to cognitive impairments. *Mol Psychiatry* 20:850–859.
- Lim JS, Kim W, Il Kang HC, Kim SH, Park AH, Park EK, Cho YW, Kim S, Kim HM, Kim JA, Kim J, Rhee H, Kang SG, Kim HD, Kim D, Kim DS, Lee JH (2015) Brain somatic mutations in MTOR cause focal cortical dysplasia type II leading to intractable epilepsy. *Nat Med* 21:395–400.
- Lin YC, Koleske AJ (2010) Mechanisms of synapse and dendrite maintenance and their disruption in psychiatric and neurodegenerative disorders. *Annu Rev Neurosci* 33:349–378.
- Louis DN, Ohgaki H, Wiestler OD, Cavenee WK, Burger PC, Jouvet A, Scheithauer BW, Kleihues P (2007) The 2007 WHO classification of tumours of the central nervous system. *Acta Neuropathol* 114:97–109.
- Machicoane M, de Frutos CA, Fink J, Rocancourt M, Lombardi Y, Gare S, Piel M, Echard A (2014) SLK-dependent activation of ERMs controls LGN-NuMA localization and spindle orientation. *J Cell Biol* 205:791–799.

- Mainen ZF, Sejnowski TJ (1996) Influence of dendritic structure on firing pattern in model neocortical neurons. *Nature* 382:363–366.
- Marrs GS, Honda T, Fuller L, Thangavel R, Balsamo J, Lilien J, Dailey ME, Arregui C (2006) Dendritic arbors of developing retinal ganglion cells are stabilized by β 1-integrins. *Mol Cell Neurosci* 32:230–241.
- Megias M, Emri Z, Freund TF, Gulyás AI (2001) Total number and distribution of inhibitory and excitatory synapses on hippocampal CA1 pyramidal cells. *Neuroscience* 102:527–540.
- Menon V, Musial TF, Liu A, Katz Y, Kath WL, Spruston N, Nicholson DA (2013) Balanced synaptic impact via distance-dependent synapse distribution and complementary expression of AMPARs and NMDARs in hippocampal dendrites. *Neuron* 80:1451–1463.
- Molyneux BJ, Arlotta P, Menezes JR, Macklis JD (2007) Neuronal subtype specification in the cerebral cortex. *Nat Rev Neurosci* 8:427–437.
- Moresco EM, Donaldson S, Williamson A, Koleske AJ (2005) Integrin-mediated dendrite branch maintenance requires Ablon (Abl) family kinases. *J Neurosci* 25:6105–6118.
- Myers JP, Gomez TM (2011) Focal adhesion kinase promotes integrin adhesion dynamics necessary for chemotropic turning of nerve growth cones. *J Neurosci* 31:13585–13595.
- Okabe S (2007) Molecular anatomy of the postsynaptic density. *Mol Cell Neurosci* 34:503–518.
- Olson A, Sheth N, Lee JS, Hannon G, Sachidanandam R (2006) RNAi Codex: a portal/database for short-hairpin RNA (shRNA) gene-silencing constructs. *Nucleic Acids Res* 34:D153–D157.
- Palop JJ, Chin J, Roberson ED, Wang J, Thwin MT, Bien-Ly N, Yoo J, Ho KO, Yu GQ, Kreitzer A, Finkbeiner S, Noebels JL, Mucke L (2007) Aberrant excitatory neuronal activity and compensatory remodeling of inhibitory hippocampal circuits in mouse models of Alzheimer's disease. *Neuron* 55:697–711.
- Papadopoulos T, Eulenburg V, Reddy-Alla S, Mansuy IM, Li Y, Betz H (2008) Collybistin is required for both the formation and maintenance of GABAergic postsynapses in the hippocampus. *Mol Cell Neurosci* 39:161–169.
- Quizi JL, Baron K, Al-Zahrani KN, O'Reilly P, Sriram RK, Conway J, Laurin AA, Sabourin LA (2013) SLK-mediated phosphorylation of paxillin is required for focal adhesion turnover and cell migration. *Oncogene* 32:4656–4663.
- Rossini L, de Santis D, Mauceri RR, Tesoriero C, Bentivoglio M, Maderna E, Maiorana A, Deleo F, de Curtis M, Tringali G, Cossu M, Tumminelli G, Bramero M, Spreafico R, Tassi L, Garbelli R (2021) Dendritic pathology, spine loss and synaptic reorganization in human cortex from epilepsy patients. *Brain* 144:251–265.
- Sabourin LA, Rudnicki MA (1999) Induction of apoptosis by SLK, a Ste20-related kinase. *Oncogene* 18:7566–7575.
- Sabourin LA, Tamai K, Seale P, Wagner J, Rudnicki MA (2000) Caspase 3 cleavage of the Ste20-related kinase SLK releases and activates an apoptosis-inducing kinase domain and an actin-disassembling region. *Mol Cell Biol* 20:684–696.
- Saito T, Nakatsuji N (2001) Efficient gene transfer into the embryonic mouse brain using in vivo electroporation. *Dev Biol* 240:237–246.
- Sakakibara A, Ando R, Sapir T, Tanaka T (2013) Microtubule dynamics in neuronal morphogenesis. *Open Biol* 3:130061.
- Schaefer AT, Larkum ME, Sakmann B, Roth A (2003) Coincidence detection in pyramidal neurons is tuned by their dendritic branching pattern. *J Neurophysiol* 89:3143–3154.
- Schmeisser MJ, Ey E, Wegener S, Bockmann J, Stempel AV, Kuebler A, Janssen AL, Udvardi PT, Shiban E, Spilker C, Balschun D, Skryabin BV, Dieck S, Smalla KH, Montag D, Leblond CS, Faure P, Torquet N, Le Sourd AM, Toro R, et al. (2012) Autistic-like behaviours and hyperactivity in mice lacking ProSAP1/Shank2. *Nature* 486:256–260.
- Sfakianos MK, Eisman A, Gourley SL, Bradley WD, Scheetz AJ, Settleman J, Taylor JR, Greer CA, Williamson A, Koleske AJ (2007) Inhibition of Rho via Arg and p190RhoGAP in the postnatal mouse hippocampus regulates dendritic spine maturation, synapse and dendrite stability, and behavior. *J Neurosci* 27:10982–10992.
- Sholl D (1953) Dendritic organization in the neurons of the visual and motor cortices of the cat. *J Anat* 87:387–406.
- Sisodiya SM, Fauser S, Cross JH, Thom M (2009) Focal cortical dysplasia type II: biological features and clinical perspectives. *Lancet Neurol* 8:830–843.
- Swiech L, Blazejczyk M, Urbanska M, Pietruszka P, Dortland BR, Malik AR, Wulf PS, Hoogenraad CC, Jaworski J (2011) CLIP-170 and IQGAP1 cooperatively regulate dendrite morphology. *J Neurosci* 31:4555–4568.
- Talos DM, Sun H, Kosaras B, Joseph A, Folkerth RD, Poduri A, Madsen JR, Black PM, Jensen FE (2012) Altered inhibition in tuberous sclerosis and type IIb cortical dysplasia. *Ann Neurol* 71:539–551.
- Thom M, Blümcke I, Aronica E (2012) Long-term epilepsy-associated tumors. *Brain Pathol* 22:350–379.
- Thome C, Kelly T, Yanez A, Schultz C, Engelhardt M, Cambridge SB, Both M, Draguhn A, Beck H, Egorov AV (2014) Axon-carrying dendrites convey privileged synaptic input in hippocampal neurons. *Neuron* 83:1418–1430.
- Tyagarajan SK, Fritschy JM (2014) Gephyrin: a master regulator of neuronal function? *Nat Rev Neurosci* 15:141–156.
- Tyagarajan SK, Ghosh H, Yévenes GE, Nikonenko I, Ebeling C, Schwerdel C, Sidler C, Zeilhofer HU, Gerrits B, Müller D, Fritschy JM (2011) Regulation of GABAergic synapse formation and plasticity by GSK3 β -dependent phosphorylation of gephyrin. *Proc Natl Acad Sci USA* 108:379–384.
- Ultamir SK, Yadav S, Hertz NT, Osés-Prieto JA, Claxton S, Burlingame AL, Shokat KM, Jan LY, Jan YN (2014) MST3 kinase phosphorylates TAO1/2 to enable myosin Va function in promoting spine synapse development. *Neuron* 84:968–982.
- van Loo KM, Schaub C, Pernhorst K, Yaari Y, Beck H, Schoch S, Becker AJ (2012) Transcriptional regulation of T-type calcium channel CaV3.2: bidirectionality by early growth response 1 (Egr1) and repressor element 1 (RE-1) protein -silencing transcription factor (REST). *J Biol Chem* 287:15489–15501.
- van Loo KM, Schaub C, Pitsch J, Kulbida R, Opitz T, Ekstein D, Dalal A, Urbach H, Beck H, Yaari Y, Schoch S, Becker AJ (2015) Zinc regulates a key transcriptional pathway for epileptogenesis via metal-regulatory transcription factor 1. *Nat Commun* 6:8688.
- Verret L, Mann EO, Hang GB, Barth AM, Cobos I, Ho K, Devidze N, Masliah E, Kreitzer AC, Mody I, Mucke L, Palop JJ (2012) Inhibitory interneuron deficit links altered network activity and cognitive dysfunction in Alzheimer model. *Cell* 149:708–721.
- Viswanatha R, Ohouo PY, Smolka MB, Bretscher A (2012) Local phosphocycling mediated by LOK/SLK restricts ezrin function to the apical aspect of epithelial cells. *J Cell Biol* 199:969–984.
- Wagner S, Flood TA, Reilly PO, Hume K, Sabourin LA, Biol MC (2002) Association of the Ste20-like kinase (SLK) with the microtubule. *J Biol Chem* 277:37685–37692.
- Wagner S, Storbeck CJ, Roovers K, Chaur ZY, Kolodziej P, McKay M, Sabourin LA (2008) FAK/src-family dependent activation of the Ste20-like kinase SLK is required for microtubule-dependent focal adhesion turnover and cell migration. *PLoS One* 3:e1868.
- Warren MS, Bradley WD, Gourley SL, Lin YC, Simpson MA, Reichardt LF, Greer CA, Taylor JR, Koleske AJ (2012) Integrin β 1 signals through Arg to regulate postnatal dendritic arborization, synapse density, and behavior. *J Neurosci* 32:2824–2834.
- Yalgin C, Ebrahimi S, Delandre C, Yoong LF, Akimoto S, Tran H, Amikura R, Spokony R, Torben-Nielsen B, White KP, Moore AW (2015) Centrosomin represses dendrite branching by orienting microtubule nucleation. *Nat Neurosci* 18:1437–1445.
- Yamauchi T (2002) Molecular constituents and phosphorylation-dependent regulation of the post-synaptic density. *Mass Spectrom Rev* 21:266–286.
- Zhang YH, Hume K, Cadonic R, Thompson C, Hakim A, Staines W, Sabourin LA (2002) Expression of the Ste20-like kinase SLK during embryonic development and in the murine adult central nervous system. *Brain Res Dev Brain Res* 139:205–215.
- Zhapparova ON, Fokin AI, Vorobyeva NE, Bryantseva SA, Nadezhkina ES (2013) Ste20-like protein kinase SLK (LOSK) regulates microtubule organization by targeting dynactin to the centrosome. *Mol Biol Cell* 24:3205–3214.